JGR Earth Surface

RESEARCH ARTICLE
10.1029/2022JF006727

A Novel Approach to Quantify Sediment Transfer and Storage in Rivers—Testing Feldspar Single-Grain pIRIR Analysis and Numerical Simulations

Anne Guyez[1,2], Stéphane Bonnet[1], Tony Reimann[2], Sébastien Carretier[1], and Jakob Wallinga[3]

[1]GET, Université de Toulouse, IRD, UPS, CNRS (Toulouse), Toulouse, France, [2]Geomorphology & Geochronology, Geographic Institute, University of Cologne, Cologne, Germany, [3]Netherlands Center for Luminescence Dating & Soil Geography and Landscape Group, Wageningen University, Wageningen, The Netherlands

Key Points:

- Feldspar single-grain post infra-red infra-red (pIRIR) luminescence data measured in modern deposits of the Waimakariri and Rakaia braided rivers (New Zealand)
- Single-grain pIRIR equivalent-dose distributions show similar along stream trends for both rivers
- A new numerical model that simulates the luminescence signal in rivers allows the estimation of transport and storage parameters from data

Supporting Information:

Supporting Information may be found in the online version of this article.

Correspondence to:

A. Guyez and S. Bonnet,
anne.guyez@get.omp.eu;
stephane.bonnet@get.omp.eu

Citation:

Guyez, A., Bonnet, S., Reimann, T., Carretier, S., & Wallinga, J. (2023). A novel approach to quantify sediment transfer and storage in rivers—testing feldspar single-grain pIRIR analysis and numerical simulations. *Journal of Geophysical Research: Earth Surface*, *128*, e2022JF006727. https://doi.org/10.1029/2022JF006727

Received 26 APR 2022
Accepted 24 JAN 2023

Abstract Quantifying sediment transport and storage in fluvial systems is fundamental for understanding the transfer of eroded materials from source to sink. Here, we investigated the potential of a combined approach using a luminescence measured in modern fluvial sediments and numerical simulations to quantify transport and storage in rivers. We acquired luminescence data at the single-grain scale on feldspar sediments of Waimakariri and Rakaia braided rivers (New Zealand) using a post infra-red infra-red stimulated luminescence protocol. We considered three metrics from the analysis of luminescence equivalent dose (D_e) distribution: the percentage of bleached and the percentage of saturated grains, and the mean D_e. All three metrics show similar longitudinal trends along both rivers. To derive quantitative information on sediment transfer from these data, we developed a numerical model that simulates the longitudinal evolution of D_e distribution of a population of grains during transport and storage in floodplains. The model considers four main parameters: the transport length of grains during floods, their resting time between successive transport events, the bleaching probability (probability of the luminescence signal to be reset due to sunlight exposure during transport or rest), and the likelihood of partial bleaching. Identification of model parameters that best reproduce natural observations allowed estimating transit time of sediments between 2.1 and 10.3 Kyr (mean of 6.9 ± 2.9 Kyr), corresponding to mean virtual transit velocity of 20–95 m.yr^{-1} (mean of 46 ± 28 m.yr^{-1}). Our study illustrates the potential of the combined single-grain luminescence and modeling approach to quantify sediment transfer in fluvial systems.

Plain Language Summary In river systems, sediments are generally transported downstream via successive steps during floods. Relatively little is known about the time it takes for sediments to travel the full distance from their upstream source to downstream. Most techniques are applicable on the scale of a few years, whereas we are dealing with transfers that occur on much longer time scales, exceeding hundred or thousand years. This transfer is complicated by the temporary storage of grains in floodplains for varying durations before remobilization and the continuation of their journey. We explore this issue by measuring the luminescence of modern sediments. Luminescence is a quantity measurable within minerals that increases when they are buried and resets when exposed to sunlight. We modeled theoretically how the luminescence signal varies alongstream in response to transport and storage along two braided rivers in New Zealand. We found that the way the signal varies in sediments of the two rivers implies a transfer time of ∼7,000 years on average, corresponding to a mean velocity of sediments over this period of ∼50 m.yr^{-1}. It will be interesting in the future to use this method to understand the transfer of sediments according to tectonic and climatic contexts and river flow patterns.

1. Introduction

The downstream displacement of sediments in rivers occurs through discrete episodes of transport during floods that alternate with periods of temporary storage in floodplains that range from the hydrological (10^{-1}–10^{2} yrs) to the geological timescale (>10^{3} yrs). Cumulative storage periods can result in a long transit time of sedimentary particles, defined as the time required for all sedimentary particles supplied to a fluvial system to reach the outlet (Repasch et al., 2020). As a consequence, input erosive signals can be delayed, damped, or even erased during their transfer from source to sink (Allen, 2008; Jerolmack & Paola, 2010; Métivier et al., 1999; Straub et al., 2020), which complicates the interpretation of sedimentary archives in terms of records of climatic or

tectonic forcing on continental surfaces (Fülöp et al., 2020; Sinclair et al., 2019). Insights in transit and storage times also have many other implications. Carretier et al. (2020) show for example, that long temporary storage of some particles may significantly increase the mean residence time of a whole population of fluvial grains, which may bias proxies measured in sediments to reconstruct paleoenvironmental conditions. Repasch et al. (2021) also show that transit time plays a key role in determining the fate of particulate organic carbon in rivers and whether the organic carbon will be, for example, oxidized and released into the atmosphere as CO_2 or efficiently transported to sedimentary sinks and buried geologically, resulting in a drawdown of atmospheric CO_2.

Many studies have addressed sediment transport during transport episodes, for example, using tracers (Vázquez-Tarrío et al., 2019). For longer timescales, the lack of dedicated methods has limited the investigation of fluvial transport on a scale integrative of these single events, at the transit time scale. Some methods have been developed or are under development, but none have yet been fully validated and are sufficiently easy to implement so that they are not commonly used yet. They are all developed for silt to sand-sized grains, so the information they can provide does not apply to the full range of the particle size distribution. Among the first attempts to approach transit times, studies based on U series isotopes measured in sediments allow to estimate comminution ages, the time since investigated grains were reduced to <63 μm in size and interpreted at the time since particles formed in the source area (Dosseto et al., 2006). These data are used to estimate the residence time of particles in the source to sink system, which is only a crude estimate of the transit time as it integrates both hillslope storage and fluvial transport. In addition to being limited to very small grain sizes, this method also presents many problems in translating the measurements into age terms (Martin et al., 2019). A second family of methods that considers the cosmogenic isotope concentrations in river sediments succeeds in providing data for filling the knowledge gap on transit times, first by providing estimates of sediment transport velocities at the millennial time-scale (Carretier & Regard, 2011; Carretier et al., 2019; Nichols et al., 2005). Recent developments complement these studies by considering novel isotopes such as in situ cosmogenic ^{14}C (Hippe et al., 2012) or meteoric (i.e., produced within the atmosphere) cosmogenic ^{10}Be (Repasch et al., 2020) and succeed in providing valuable information respectively on storage in floodplains and transit times. The paired ^{14}C-^{10}Be method considers the ratio of in situ, short-lived ^{14}C to longer-lived cosmogenic isotopes ^{10}Be, measured in fluvial sediments. This method allows estimating storage over 10^3–10^4 yr time scale, provided that the initial ratio of short- to long-lived isotopes is known. This prerequisite can be an issue in source areas where soil mixing is important or where the erosion rate has changed recently (Hippe et al., 2012). Repasch et al. (2020) recently estimated transit times by measuring upstream to downstream accumulation of cosmogenic ^{10}Be of meteoritic origin ($^{10}Be_m$) in the suspended sediment load, $^{10}Be_m$ being adsorbed on mineral surfaces and incorporated into the secondary mineral coatings. This method is quite complex to implement because it requires establishing a full, depth-integrated, inventory of $^{10}Be_m$ in the sediment load and estimating potential loss in the floodplain; however, it allows estimating transit times over 10^3–10^5 yr time scale. Repasch et al. (2020) then provide detailed estimates of transit time for the Rio Bermejo (Argentina), being of 8.4 ± 2.2 Kyr for a 1,220 km-long river, corresponding to a mean virtual velocity of sediment of ∼145 m yr^{-1}. They also document a higher virtual velocity in the upstream braided segment of this river than in its downstream, meandering one.

A number of recent studies have suggested that insights on sediment transfer could also be gained by considering the natural luminescence signals of fluvial silt and sand sediments (see synthesis in Gray et al. (2019)). This luminescence signal is reset by light exposure, and accumulates through absorption of energy from the background ionizing radiation. Luminescence is widely used to determine the burial age of sediments, but could also provide complementary information on sediment transport, regarding for example, characteristic transport length or storage duration of particles, or frequency of flooding events (Gray & Mahan, 2015; McGuire & Rhodes, 2015a, 2015b). Natural luminescence signals of modern sediments have been shown in a few examples to decrease downstream (Gray et al., 2018; Guyez, Bonnet, Reimann, Carretier, & Wallinga, 2022; McGuire & Rhodes, 2015a; Stokes et al., 2001), which implies that the related signals are progressively reset (zeroing) by exposure of grains to sunlight during their transit in the fluvial system. McGuire and Rhodes (2015b) show that a simple model of progressive signal resetting linked to successive floods can reproduce the observed longitudinal trends of feldspar luminescence signals from modern sediments of the Mojave River. They proposed for the first time that such data could be used to extract the virtual velocity of sediments from the luminescence of modern deposits and proposed a first model for this purpose. Gray and Mahan (2015) considered two end members theoretical models that could result in the longitudinal decrease in luminescence signals: (a) progressive zeroing of the signal by sunlight exposure of the grains at bar surfaces in the floodplain in between floods ("episodic flood

case") and (b) continuous zeroing during transport of sediments due to subaqueous light exposure ("continuous flow case"). Based on the continuous flow model, Gray et al. (2018) estimated that the zeroing of particle luminescence occurred over a distance of 15–23 km in the South River (USA). The authors combined this with an independent estimate of the storage timescale of the particles in the floodplain (~8 Kyr) from the literature to derive a mean virtual velocity of particles of 1.8–2.8 m yr^{-1}.

Here, we propose that the luminescence of modern sediments is a valuable tool for constraining not only fluvial transport but also storage and transit times in fluvial systems. For this purpose, we acquired a comprehensive luminescence data set of modern sand sized sediments along two New Zealand braided rivers. Building on earlier work by McGuire and Rhodes (2015b), Bonnet et al. (2019), Guyez, Bonnet, Reimann, Carretier, and Wallinga (2022), we measure luminescence signals of individual feldspar grains. The specificity of our approach is that we use several metrics based on the single-grain equivalent dose (D_e) distribution to derive proxies for transport and storage processes. Our new single-grain data are combined here with results from a newly developed numerical model that simulates the gain and loss of the luminescence signal of sediments in response to episodic fluvial transport and storage. The combination of field data and modeling allows us to estimate the characteristic transport length of particles and their mean temporary storage time in the floodplain and finally to evaluate the transit time and virtual velocity of grains in the two studied rivers.

2. Background: Luminescence of Fluvial Sediments

Luminescence is a property that is commonly used for dating Quaternary deposits: Optically Stimulated Luminescence (OSL) for quartz (Murray & Roberts, 1997) or Infrared-Stimulated Luminescence (IRSL) for feldspar grains (Reimann et al., 2012). When deposited, mineral grains are constantly exposed to ionizing radiation, from the mineral itself, surrounding material and cosmic rays when close to the Earth's surface, at a rate referred to as dose rate (in Gy.Kyr^{-1}). These radiations create charge that may be trapped in defects of the crystal lattices potentially until a saturation state is reached with no further accumulation (some traps are actually unstable and never get to saturation). The absorbed radiation dose of grains, referred to as the D_e, can be determined by comparing the natural luminescence signal to laboratory-induced ones through their optical or thermal stimulation (Aitken, 1998; Preusser et al., 2008). When the mineral is exposed to heat or light, a process called bleaching, charges are evicted from their traps and the quartz OSL signal, or feldspar IRSL signal, is reset. Complete bleaching under subaerial conditions takes some seconds for quartz and several minutes for feldspar (Godfrey-Smith et al., 1988; Murray et al., 2012; Smedley & Skirrow, 2020). For elevated temperature post infra-red infra-red (pIRIR) signals measured on K-feldspar, complete bleaching can take up to several days of full daylight exposure (Kars et al., 2014; McGuire & Rhodes, 2015a). Subaqueous bleaching is slower, due to reduced intensity and light spectrum in water, especially when sediment concentration and turbidity are high (Berger, 1990; Davies-Colley & Nagels, 2008; Ditlefsen, 1992).

Although several studies have shown near-complete bleaching in downstream reaches of major rivers (Chamberlain et al., 2018; Wallinga, 2002), heterogeneous bleaching of quartz and feldspar is common for smaller systems and upstream reaches (Bonnet et al., 2019; Chamberlain & Wallinga, 2019; Wallinga, 2002). Such heterogeneous bleaching may be due to attenuated bleaching efficiency in turbid flow (Ditlefsen, 1992), luminescence signal bleachability (Kars et al., 2014), fast erosion rates (Bonnet et al., 2019), alongstream supply of unbleached grains (Guyez, Bonnet, Reimann, Carretier, & Wallinga, 2022), or dose regeneration due to temporary storage in floodplains (Goehring et al., 2021). The few studies that have investigated D_e variations of modern sediment alongstream (Gray et al., 2018; Guyez, Bonnet, Reimann, Carretier, & Wallinga, 2022; McGuire and Rhodes, 2015a, 2015b; Stokes et al., 2001) document longitudinal decreases in mean D_e, interpreted as the signature of a progressive D_e reduction of the sediment mix due to cumulative bleaching. Nearly all these studies are based on measurements made on the whole populations of multiple grain aliquots, which limit thorough understanding of actual bleaching, lateral supply, or regenerating mechanisms accounting for the observed longitudinal decrease in D_e. To tackle this problem, some authors used several feldspar luminescence signals by stimulating samples under Multiple Elevated Temperatures (MET) protocol (McGuire and Rhodes, 2015a, 2015b; Reimann et al., 2015; Rhodes & Leathard, 2022). Because of contrasted bleaching rates, these different signals yield complementary information for understanding alongstream transport. In some cases, these MET protocols have been used for single-grains, yielding multiple signals from the same grain (e.g., McGuire & Rhodes, 2015b). Another approach is to use single-grain D_e distributions of heterogeneously bleached samples. It consists of measuring D_e for each grain

independently (see Reimann et al. (2012) for feldspar), allowing for instance to identify bleached grains within a whole grain population. Applying a single-grain protocol to investigate bleaching related to fluvially transported sands is thus potentially a powerful way to advance our knowledge of processes related to sediment transport (Bonnet et al., 2019; Guyez, Bonnet, Reimann, Carretier, & Wallinga, 2022; McGuire & Rhodes, 2015b).

3. Luminescence of Modern Deposits of the Waimakariri and Rakaia Rivers

3.1. Setting

The Waimakariri and Rakaia rivers originate from the central part of the Southern Alps of New Zealand and flow eastward from the Southern Alps Foothills (SAF) to the Pacific Ocean through the Canterbury Plains (CP) where they form wide gravel-bed braided rivers (Figure 1). The Southern Alps constitute a tectonically active orogen that arises in response to the ongoing collision between the Australian and Pacific plates (Kamp & Tippett, 1993; Norris & Cooper, 2001). It is actively uplifting and eroding, with exceptionally high rates of exhumation and erosion, in particular in the western side of the orogen where they locally exceed 10 mm yr^{-1} (Herman et al., 2009; Hovius et al., 1997). Although less evident, exhumation in the eastern side of the Southern Alps drained by the Rakaia and Waimakariri rivers still reaches several mm yr^{-1} (Adams, 1980), while geodetic data indicate active surface uplift at similar rates (Beavan et al., 2010). Bedrock of the mountainous area of the Waimakariri and Rakaia catchments is dominated by quartz-feldspathic sandstones interbedded with siltstones and mudstones referred to as Triassic Greywackes of the Rakaia Terrane (Cox & Barrell, 2007). These areas have glaciated several times during the Quaternary (Barrell et al., 2011). At the front of the Alps, up to 650 m of glaciofluvial sediments accumulated in the CP during the Quaternary (Browne & Naish, 2003), the most recent ones having accumulated during the Last Galcial Maximum (LGM, 37–18 Kyr: Rowan et al., 2012). The Waimakariri and Rakaia rivers have a braided pattern both in the large glacial valleys of the SAF and in the CP, except at the transition between these two domains where they flow in narrow gorges (Figure 1a). Both rivers widen important as they exit these gorges and are currently entrenched into LGM deposits that form the surface of the CP. Entrenchment into the CP reaches a maximum near the SAF, being of ∼100 m, and it gently decreases downstream.

The mean catchment-scale annual precipitation is 3,000 mm on the Rakaia and of 1,900 mm on the Waimakariri (Griffiths, 1981). The Rakaia drains a 3,065 km^2 catchment. Its average flow is about 200 $m^3\ s^{-1}$ with peaks that can reach 2,000 $m^3.s^{-1}$ during floods (Table S1 in Supporting Information S1; Griffiths, 1981). The Waimakariri drains a 3,200 km^2 catchment. Its average annual flow is 120 $m^3.s^{-1}$ with a peak at 1,700 $m^3\ s^{-1}$ (Table S1 in Supporting Information S1; Griffiths, 1981). These two rivers transport massive amounts of sediments, of respectively 4.15 and 3.14 Mt yr^{-1} for Rakaia and Waimakariri (Table S1 in Supporting Information S1; Hicks et al., 2011), among the highest worldwide sediment yields given their catchment size (1,641 and 1,669 t $km^{-2}\ yr^{-1}$: Griffiths, 1981). The two rivers have a similar bed slope gradient, of 0.004–0.005 m m^{-1} (Mosley, 1983). No significant tributaries connect to these rivers in the CP, making them interesting natural laboratories to test innovative ways for investigating sediment transport.

3.2. Sampling and Luminescence Measurements

We measured the luminescence signal of single-grain of feldspar (212–250 μm) of 14 samples of modern sediment of the Waimakariri and Rakaia using the post-Infrared IRSL (pIRIR) Single Aliquot Regenerative dose (SAR) protocol of Reimann et al. (2012) at 175°C ($pIRIR_{175}$; see Text S1 and Table S2 in Supporting Information S1). Samples were collected in February 2020 during low flow conditions allowing access to sand bars in the active floodplain (Figures 1c and 1d; Figures S1 and S2 in Supporting Information S1). On each river, we took two samples upstream of the gorges and four (Rakaia) to six (Waimakariri) in the CP, distributed from the gorge output to the river mouth (Figure 1a). From 200 to 400 individual feldspar grains were measured for each sample. All samples were prepared and analyzed at the Netherlands Center of Luminescence Dating using an automated Risø thermoluminescence/OSL reader (DA 15) fitted with a dual (infrared and green) laser single-grain attachment (Bøtter-Jensen et al., 2003). In the adopted SAR procedure, regenerative doses between 0 and 240 Gy are applied to generate a test dose corrected dose response curve. Natural pIRIR signals are projected on this curve to obtain D_e values. Anomalous fading may affect the $pIRIR_{175}$ signal, although its impact was shown to be limited in previous studies in the Rangitikei catchment (northern Island NZ, Bonnet et al., 2019; Guyez, Bonnet,

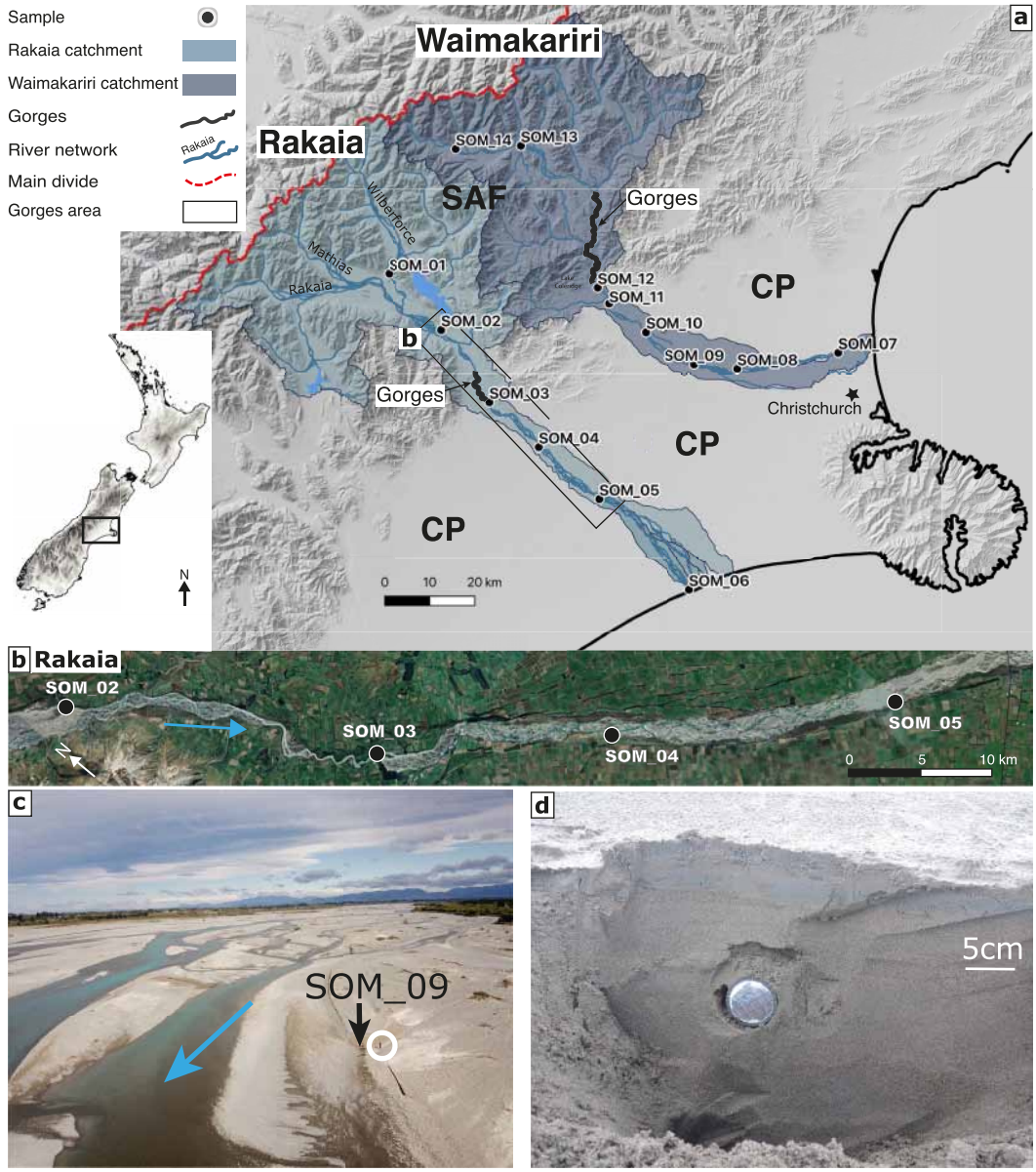

Figure 1. (a) Map of the Rakaia and Waimakariri catchments (South Island, New Zealand; see inset map) with localization of the samples for luminescence analysis. Both rivers are braided in their upstream (Southern Alps Foothills (SAF)) and downstream (Canterbury Plains (CP)) reach. Note the presence of a gorge section at the transition between the SAF and the CP and the absence of tributaries in the CP sections. (b) Google Earth view (CNES/Airbus) showing the gorges and a braided section of the Rakaia river in the CP (see location on panel (a)). (c) Aerial view of the Waimakariri river at the location of sample SOM_09. Upward view to the North West. With the Southern Alps in the back. (d) Close view of sample SOM_09. Samples were taken in the modern floodplain by hammering PVC tubes into sand bodies.

Reimann, Carretier, & Wallinga, 2022). No fading measurements or corrections were used for this study, as the pIRIR data is not used for estimating burial ages. Additional details on luminescence measurements and tests are provided in Text S1 in Supporting Information S1.

3.3. Longitudinal Trends in Luminescence Signals

From the 200 to 400 individual feldspar grains measured in each sample, 75 to 199 provided sufficient signal to estimate D_e (Table 1). We analyze the longitudinal distribution of single-grain D_e by considering three subgroups (Figure 2).

Table 1
Luminescence Data From the Rakaia and Waimakariri Rivers

River	Sample	Distance from gorges output (km)	Total measured grains	Grains that gave a measurable signal	Saturated grains (%)	Grains with D_e < 10 Gy (%)	Mean D_e (Gy)
Rakaia	SOM_01	−42.2	189	180	6	40	20.95 ± 2.04
	SOM_02	−22.5	117	116	3	45	27.13 ± 4.74
	SOM_03	0	122	108	16	45	19.96 ± 3.50
	SOM_04	17.2	102	96	10	42	28.41 ± 4.17
	SOM_05	35.0	96	95	1	52	15.64 ± 2.19
	SOM_06	65.0	120	120	2	68	10.35 ± 1.36
Waimakariri	SOM_14	−69.8	125	113	16	36	43.01 ± 6.04
	SOM_13	−53.6	199	172	17	31	37.17 ± 4.21
	SOM_12	0	116	106	15	22	44.95 ± 6.22
	SOM_11	5.1	75	75	1	99	0.85 ± 0.05
	SOM_10	17.7	174	165	8	35	32.09 ± 3.68
	SOM_09	31.6	167	163	3	37	35.46 ± 3.73
	SOM_08	42.0	140	136	4	48	20.88 ± 2.68
	SOM_07	65.6	112	112	2	68	9.75 ± 1.20

Note. Note that SOM_11 was considered as an outlier and removed from the study as it shows a mean D_e close to 0. This sample has possibly been light exposed accidently during sampling or preparation.

First, grains with a D_e below a threshold of 10 Gy are considered as bleached. This threshold is based on residual D_e measured after 65 hr of light exposure in a solar simulator (see Figure S3 in Supporting Information S1; residual D_e values between 0 and 17 Gy for the Waimakariri grains and 0 and 10 Gy for the Rakaia). These residual doses presumably correspond to a hard-to-bleach component (Kars et al., 2014). Considering the 10 Gy threshold yields percentages of bleached grains from 22% to 68% on the Waimakariri and 42%–68% on the Rakaia (Table 1). As the threshold is somewhat arbitrary, we tested whether similar results would be obtained with lower (e.g., 5 Gy) of higher (e.g., 20 Gy) threshold. Although the percentages of bleached grains are different with these thresholds, the relative downstream trends, however, remain similar (Figure S4 in Supporting Information S1).

We define a second group of grains with very high D_e close to a saturation threshold (Figure 2). Such a grain is defined as saturated when its natural signal is too elevated to be projected on dose response curves or is above a $2*D_0$ criterion (Wintle & Murray, 2006) where D_0 is a characteristic constant in the exponential fitting of the dose response curve that is determined for each grain (see Figure S5 in Supporting Information S1; see also Guyez, Bonnet, Reimann, Carretier, & Wallinga, 2022). Here, these saturated grains represent 1%–17% of the grains of the Rakaia and Waimakariri samples (Table 1) and have on average a D_e above 350 Gy ($2*D_0$ criterion).

Considering a common dose rate of ∼3–4 Gy.Kyr^{-1} (Rowan et al., 2012), these saturated grains yield apparent ages of at least 90–100 Kyr, and thus are mainly sourced from the bedrock or old glacial or fluvial deposits without posterior significant bleaching. Finally, the third subgroup contains the other grains that are not bleached nor saturated, that is, having D_e between 10 and 350 Gy (Figure 2). These grains may be partially bleached grains that yielded a saturated signal prior to erosion, or they may originate from deposits of intermediate age with unsaturated signals.

The longitudinal patterns of bleaching (% of bleached grains) on both rivers are very similar (Figure 3). The two data sets show a strong increase in the proportion of bleached grains from the gorge output to the river mouth, where almost 70% of the grains are bleached in the two rivers. These data give mean bleaching gradients of 0.7% and 0.4% km^{-1} 1 for Waimakariri and Rakaia, respectively. In contrast, the amount of saturated grains decreases downstream in the CP for both rivers, from ∼15% at the gorge outputs to 1%–2% near the river mouths (Figure 3). We complement these data with alongstream analysis of the mean D_e of the samples, computed considering only unsaturated grains. As for saturation, the mean D_e decreases downward for both rivers in the CP (Figure 3).

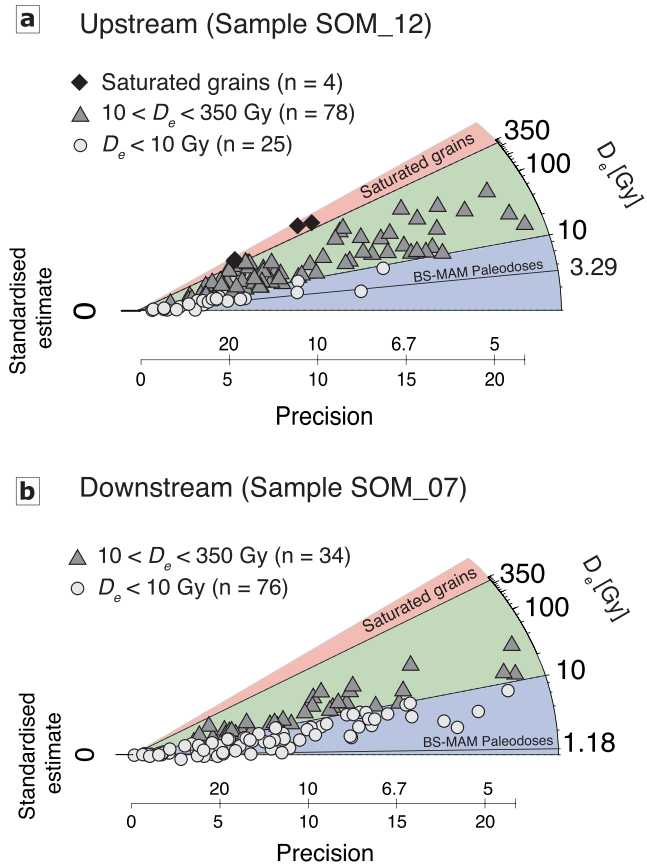

Figure 2. Radial plots of samples SOM 12 (a) and SOM 07 (b) taken respectively upstream and downstream the course of the Rakaia River in the Canterbury Plains (see location on Figure 1a). Each symbol shows the measured equivalent dose (D_e) of a single feldspar grain. Colors and shape differentiate the three types of grains considered in the study: saturated grains (D_e > 350 Gy; red field), bleached grains (D_e < 10 Gy; blue field) and grains in-between (green field). Lines in blue domain indicate the Bootstrapped-Minimum Age Model (BS-MAM) paleodoses. Note that for each sample, some saturated grains for which it was not possible to estimate D_e (see text) is not shown on the diagrams. The comparison of the two diagrams illustrates the better bleaching of samples downstream.

We characterized the longitudinal trends in bleaching, saturation and mean D_e by using the following exponential fits:

$$y = 100 - a.e^{\frac{-x}{L_{Bl}}} \quad \text{for bleaching} \tag{1}$$

$$y = y_0 - a.e^{\frac{-x}{L_{sat}}} \quad \text{for saturation} \tag{2}$$

$$y = y_0 - a.e^{\frac{-x}{L_{mean}}} \quad \text{for mean } D_e \tag{3}$$

with x the downstream distance, L_{Bl}, L_{sat}, and L_{mean} the characteristic length of longitudinal variations, y_0 the intercept and a a constant. Each characteristic length is very similar for the two rivers (Figures 3a and 3b). In the following section, we will consider values of L_{Bl}, L_{sat}, and L_{mean} from a fit on a data set that combines the data from both rivers (Figure 3c), which is conceivable because of the geographic proximity and high similarity of the two rivers. When merged together, fit on these data give values of L_{Bl} = 106.12 ± 29.33 km, L_{sat} = 24.93 ± 3.54 km, and L_{mean} = 72.29 ± 32.35 km (Figure 3c). In line with previous studies (Gray & Mahan, 2015; McGuire and Rhodes, 2015a, 2015b), we assume that these longitudinal trends in signals reflect the transport and storage of grains in the fluvial systems. To test this hypothesis, we built a model that simulates single-grain luminescence signals during transport and we will use the values of characteristic lengths for evaluating the performance of the model.

4. A Simple Model to Simulate Along Stream Luminescence Signals

We built a simple model for simulating the evolution of single-grain luminescence signals of fluvial sediments to evaluate how transport influences the longitudinal distribution of D_e and then whether we can inverse observed D_e trends to infer sediment transfer. The model (Figure 4a) considers the input of 400 grains upstream a fluvial reach and their subsequent course downstream. Half of the grains are assigned an initial dose of 50 Gy, which is about the average dose of the Waimakariri and Rakaia grains entering the CP, and the other half have a saturated signal, chosen at 500 Gy here. For the sake of simplification and in order to apprehend in priority the role of transport parameters, we do not further consider along stream supply of additional grains from river flanks, channel bed and tributaries in the model. This assumption is justified for the systems of interest, as the Waimakariri and Rakaia rivers are only slightly entrenched in the CP, without any connection of tributaries.

In the model, alternating steps of transport, deposition and storage are repeated for each input grain until it reaches the river mouth. This mimics episodical transport of grains during successive floods. First, the grain is transported over a distance (Figure 4a) defined randomly using an exponential distribution, consistent with studies on grains travel length distribution (Lajeunesse et al., 2010). This distribution is centered here on a mean value ($<L_T>$) that we have varied from 0.2 to 20 km. $<L_T>$ represents the average distance of transport of grains in the flow from their erosion to their redeposition and may be related to the sediment transport length used in landscape evolution models (Carretier et al., 2020; Davy & Lague, 2009; Davy et al., 2017; Guerit et al., 2019). For convenience, we ran the model for river lengths of 100–400 km depending on $<L_T>$, because for short $<L_T>$, the luminescence signals quickly stabilize longitudinally.

After each transport event, grains stop during a period of time, hereafter referred to as the Resting time R_t (Figure 4a), defined randomly using a Pareto distribution, consistent with recent observations that the resting

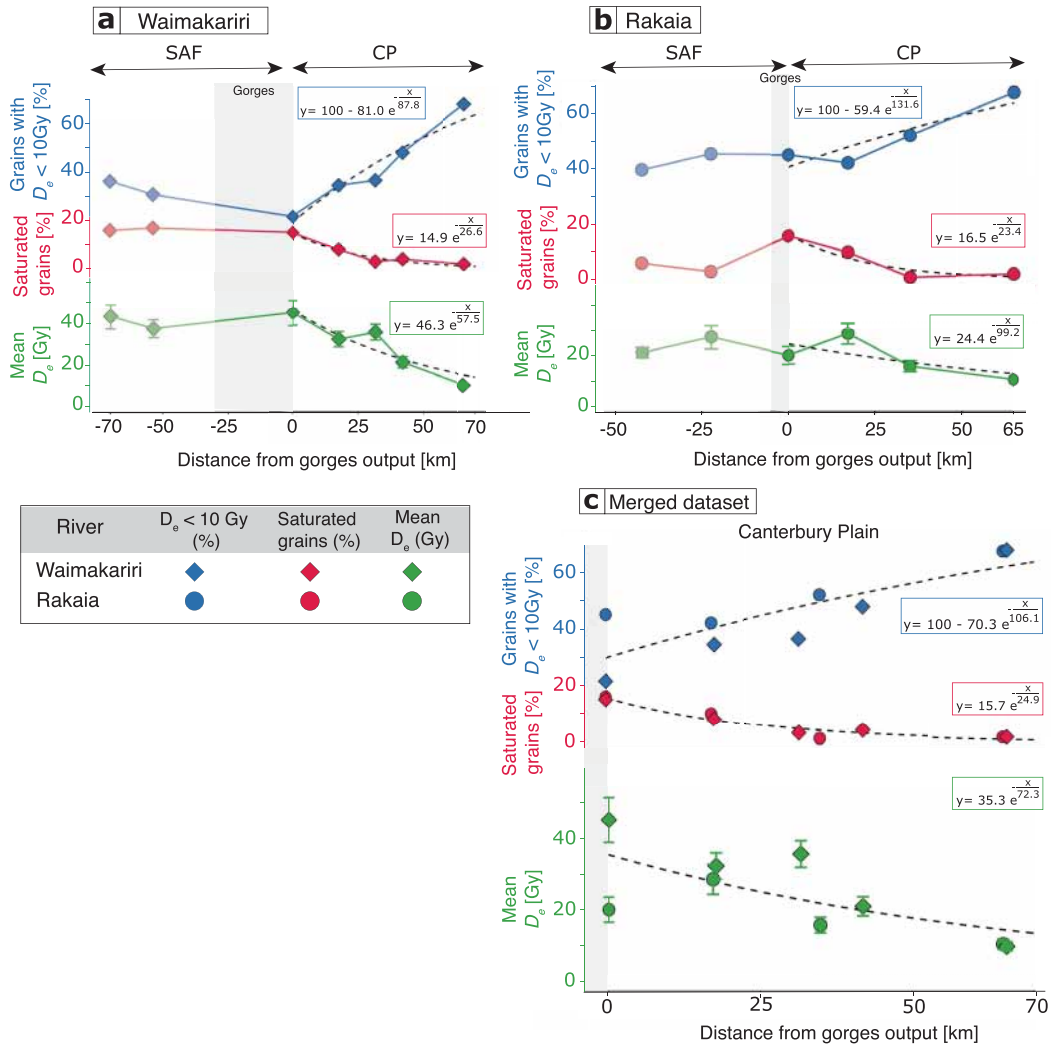

Figure 3. Along stream luminescence data. Longitudinal trends of percentages of bleached (D_e < 10 Gy; blue) and saturated (D_e > 350 Gy; red) grains and of mean D_e of modern sediments of the Waimakariri (a) and Rakaia (b) rivers. Southern Alps Foothills (SAF) and Canterbury Plains (CP) respectively indicate river courses in the SAF or CP (see Figure 1a). Note that the origin of distances has been chosen at the boundary between these two domains. Dashed lines show exponential fit on data in the CP. Graphs in (c) show combined data for both rivers for the CP section.

time of particles in rivers is heavily tailed (Bradley, 2017). The corresponding probability density function has the form:

$$\mathrm{pdf}(< R_t >, \alpha) = \frac{\alpha m^{\alpha}}{< R_t >^{\alpha+1}} \tag{4}$$

with α the shape parameter and m the scale parameter that represents the smallest value that the distributed random variable can take. The lower the α value, the longer the tail of the distribution of R_t, that is, the higher the probability to have grains with high R_t. α values of 2 and 3 were tested and do not significantly affect the results (Figure S6 in Supporting Information S1) and we used a value of 2 in the following. R_t may correspond to a rest period during two successive floods or to storage in the floodplain due for instance to river wandering. We used mean values of $<R_t>$ between 2 and 1,000 years, considering that the lower value would represent transport and rest linked to flood at the annual-scale, while higher values could correspond, for example, to temporary abandonment of part of the floodplain due to river wandering. We did not use $<R_t>$ longer than 1,000 years because it induces extremely long burial times of grains in the floodplain. As we will discuss below, even $<R_t>$ > 200 yrs are already very high in the context here.

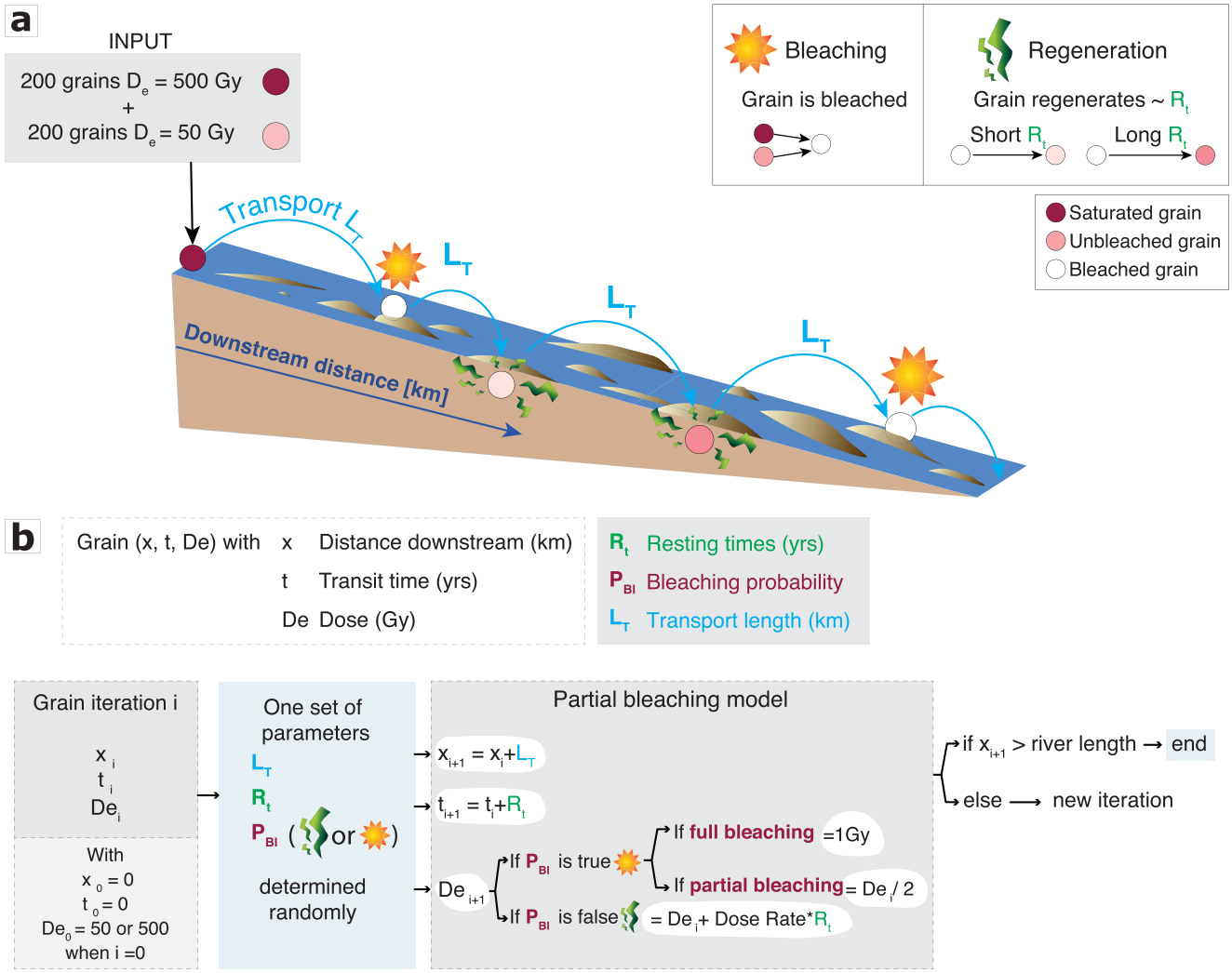

Figure 4. (a) Schematic representation of the model operations in a simulation run and (b) schematic representation of the algorithm of treatment of each grain that is computed by the model.

In association with the two successive steps of transport and rest, a Bernoulli test of probability P_{Bl} is used to define whether the grain is bleached (Figure 4a). In the model, bleaching due to sunlight exposure may occur implicitly in the water column during transport or at the surface of the floodplain during R_t. Nevertheless, because of light attenuation in turbid flows (Ditlefsen, 1992), the effectiveness of bleaching during transport is questioned and it has been proposed that the cumulative downward bleaching is dominated by bleaching at the surface during R_t, as in the episodic flow model of Gray and Mahan (2015). This parameter is qualitatively similar to the bleaching efficiency of Gray et al. (2018). However, to the best of our knowledge, the range of values that P_{Bl} could take is largely unknown. As it is defined here, this probability includes a large variety of processes which are themselves poorly constrained, such as light exposure and bleaching of particles in turbid and turbulent water flow (Ditlefsen, 1992; Mey et al., 2020), variations in sunlight intensity during rainfall events (Gray et al., 2018), variations of grain exposure due to eolian deflation (Laity, 2003; Liu & Coulthard, 2017), biological activity in floodplains (Trimble & Mendel, 1995), etc. which all could be first order here. We consequently considered a large range of P_{Bl} values from 0.01 to 0.5 for simulating respectively partial to complete bleaching conditions. Higher values would simulate a bleaching efficiency that would be inconsistent with observed poor bleaching in modern deposits of the Waimakariri and Rakaia rivers (Table 1).

We will additionally consider two ways of modeling bleaching in relation to P_{Bl} depending on whether the luminescence signals of light-exposed grains are completely reset (full bleaching model) or only partially for part

of the grains (partial bleaching model). Full bleaching conditions are likely, for example, for grains that are exposed at the surface of bars in the floodplain during R_t, because of the range of values used for $<R_t>$ (years), much longer than the time necessary to fully bleach the signal (some minutes to tens of minutes). Under full bleaching conditions, the dose of a light-exposed grain in the model decreases instantaneously to 1 Gy, regardless of its initial dose. Note that we chose a dose of 1 Gy for bleached grains instead of 0 Gy to take into account the hard-to-bleach components of pIRIR signals (Kars et al., 2014). Under partial bleaching conditions, a light-exposed grain (following the probability P_{Bl}) can be either fully bleached as previously (and its D_e is reset to 1 Gy) or partially bleached, resulting in a reduction of its D_e by a factor of two (Figure 4b). We applied partial bleaching to 80% of the light-exposed grains and full bleaching to 20%. The estimate that 80% of the grains are partially bleached and 20% are well bleached, is based on two independent lines of evidence. First, McGuire and Rhodes (2015b) estimate that all grains are partially bleached in the Mojave River (USA). The Mojave River is ephemeral and sediment transport mainly occurs during decadal extreme flood events. On the contrary, we deal here with rivers with a very different hydrologic regime, where flow is permanent with pluriannual floods. Therefore, we expect better bleaching conditions in our rivers. Hence, we assume that part of the grains is fully bleached during fluvial transport and temporary subaerial exposure on banks. Second, we tested our methods with different percentages of grains being partly bleached. We found a limited effect on modeling results when assuming 30% of the grains partially bleached, and then settled for a percentage of 80%. Moreover, we assume that partial bleaching causes a 50% reduction in the equivalent dose. We acknowledge that additional work is needed to improve these estimates of river-specific bleaching characteristics, for example, using luminescence data on modern deposits from the system.

Finally, if P_{Bl} in the model indicates that a grain is not light-exposed during a given event of transport and deposition, it implies that it is not exposed at the surface during R_t, then its signal grows proportionally to the environmental dose rate during its storage time in the floodplain (Figure 4a). Here, we used a common dose rate of 3 Gy.Kyr^{-1} (Rowan et al., 2012).

We show in Figures 5a and 5b some chronicles of grain displacement and temporary rest as well as the related time-evolution of their D_e. In the following, to foster comparison of natural and simulated data, results from our simulations are analyzed as natural data, by using bleaching and saturation thresholds of 10 and 350 Gy, respectively.

5. Modeling Results

5.1. Influence of Input Parameters on Longitudinal Trends of Luminescence Signals

Our model simulates various longitudinal trends of the investigated signals linked to transport and deposition of individual grains (Figure 6), with patterns consistent with natural data, where the percentage of saturated grains and the mean D_e decrease downstream, while the proportion of bleached grains increases. We cross-tested the effect of $<L_T>$, P_{Bl}, and $<R_t>$ on these patterns and observed that their combinations resulted in a large range of L_{Bl}, L_{sat}, and L_{mean} values, from less than 1 km to more than 1,000 km in extreme cases. These latter values are observed for very long transport distances $<L_T>$, in association with small chances of light exposure (low P_{Bl} value). This results in extreme solutions that clearly do not apply to the fluvial systems studied here. In the following section, we will first present results from modeling under full bleaching conditions and then consider the effect of partial bleaching.

5.1.1. Full Bleaching Conditions

In all our 1,036 simulations under full bleaching conditions, the proportion of grains in saturation decreases downstream due to successive bleaching events, with L_{sat} values from 1 to 2,475 km depending on model parameters. Short transport lengths $<L_T>$ favor bleaching opportunities over short distances and thus result in more rapid downward decrease in saturation that is, in lower values of L_{sat} (Figure 6a). By definition, an increasing P_{Bl} value also increases bleaching opportunities and acts in a similar way (Figure 6a). We do not observe any influence of $<R_t>$ on the saturation trends (see saturation trends for $<R_t>$ values of 2 or 200 yr in Figure 6a), which is probably due to the range of $<R_t>$ used that, combined with the dose rate of 3 Gy.Kyr^{-1}, do not cause burial long enough to overpass the saturation threshold of a majority of particles. We estimate that the saturation trends would be affected by burial only for long-time storage of grains in the floodplain corresponding to $<R_t>$ values higher than thousands of years in our model.

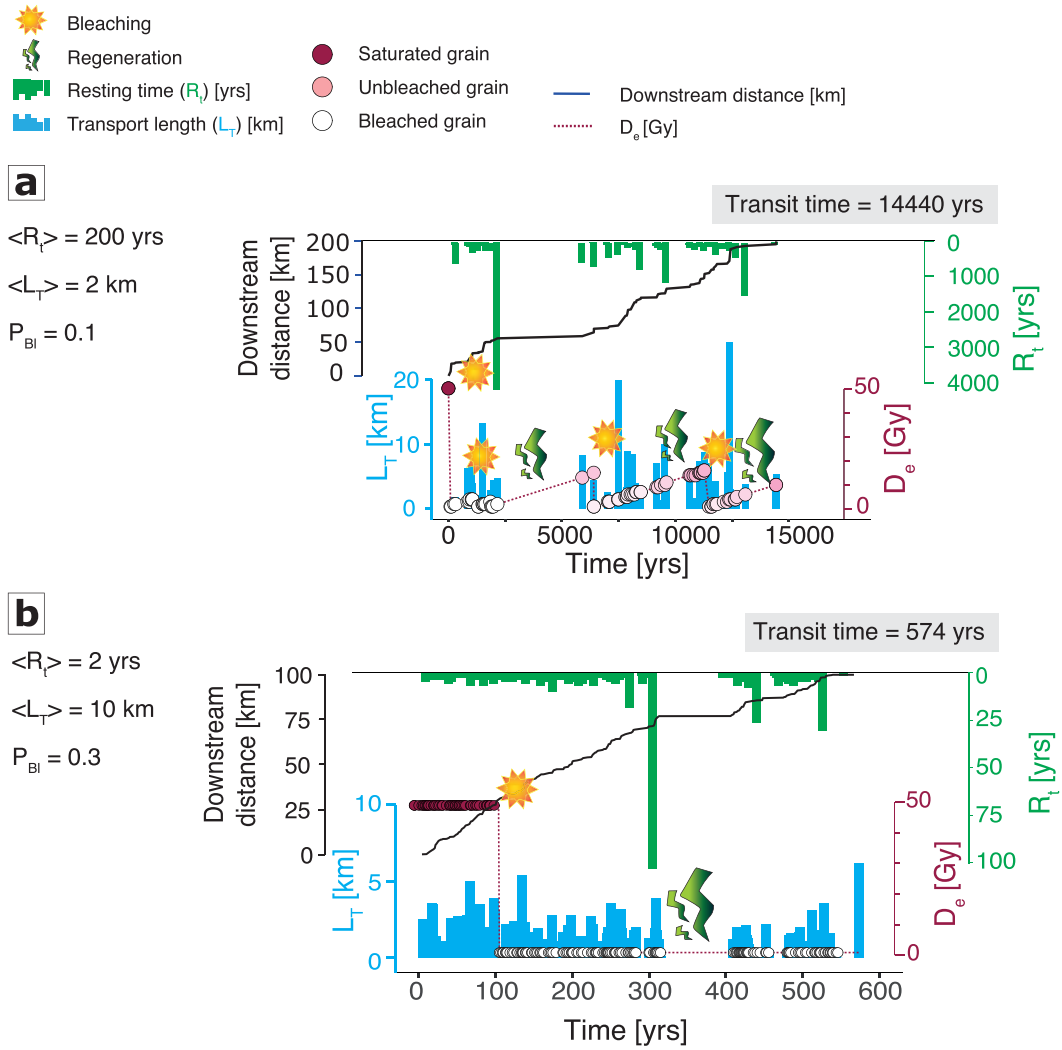

Figure 5. Graphs in (a) and (b) show two examples of chronicles for a grain in a simulation with $<R_t> = 200$ yrs, $<L_T> = 2$ km, and $P_{Bl} = 0.1$ (in a) and with $<R_t> = 2$ yrs, $<L_T> = 10$ km and $P_{Bl} = 0.3$ (in b). Cyan bars show successive elementary displacement of the grain, with cumulative displacement shown in blue (solid line). Green bars show the duration of rest of the grain in the floodplain between the two transport events. The cumulative rest time defines the transit time. Pinkish circles and red dotted lines show time-evolution of the equivalent dose D_e of the grain. It grows proportionally to R_t if the grain is buried during rest (not bleached), and decreases if bleached due to exposure to sunlight. Results shown here are under full bleaching conditions (see text).

The percentage of bleached grains (which are defined as the grains with a D_e < 10 Gy), generally increases downstream due to the successive transport episodes (Figure 6a). The corresponding L_{Bl} values vary from 1 to 1,745 km, with strong longitudinal increase in number of bleached grains (*i.e.*, low L_{Bl}) being enhanced by low $<L_T>$ and high P_{Bl}. For short values of $<R_t>$ (Figure 6a), longitudinal trends of bleaching mirror saturation, with 100% of the grains being bleached downstream. However, for higher $<R_t>$ values, signal regeneration of some grains during burial with long R_t compensates the longitudinal bleaching and the proportion of bleached grains equilibrates and forms a plateau at a lower level than 100% (Figure 6a).

The mean D_e decreases downstream with L_{mean} values from 1 to 1,269 km in our simulations. As for saturation, small transport length $<L_T>$ and/or high bleaching probability P_{Bl} result in a sharper decrease in mean D_e and lower L_{mean} (Figure 6a). However, in contrast with saturation that is not affected by R_t, the mean D_e decrease is frequently affected by temporary storage of grains, especially for long R_t. This results in a slower decrease in mean D_e and higher L_{mean}. However, even in simulations with long $<R_t>$, the effect of regeneration during burial can be annihilated if bleaching is very efficient (high P_{Bl}, Figure 6a).

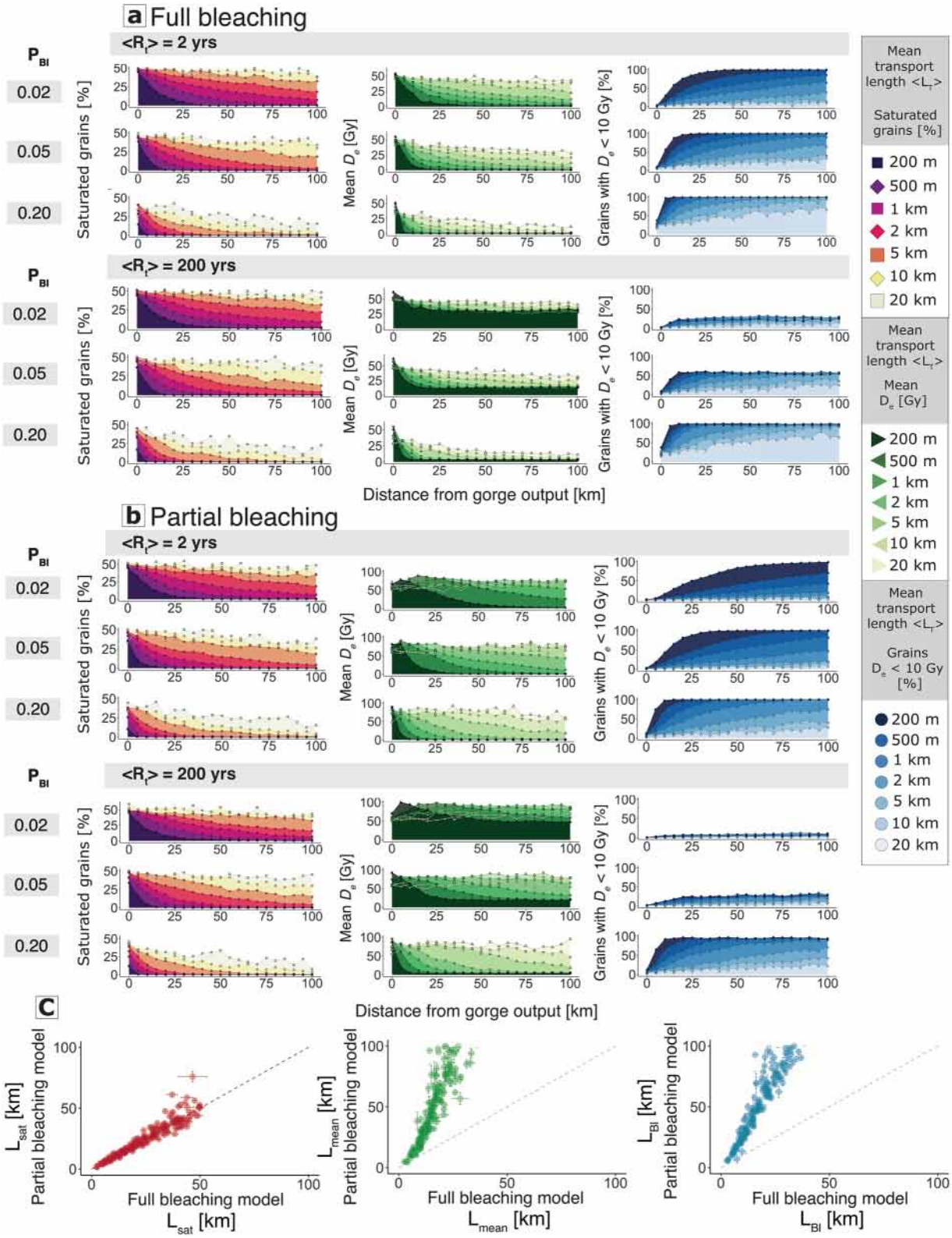

Figure 6. Graphical representation of simulation results showing the longitudinal evolution of the percentage of saturated grains (D_e > 350 Gy; left column), mean D_e (middle column) and percentage of bleached grains (D_e < 10 Gy; right column) for various mean transport length $<L_T>$ (color gradient), bleaching probability P_{BI} (rows) and resting times $<R_T>$ of 2 (top) and 200 years (bottom) under full (a) or partial (b) bleaching conditions. (c) Comparison of characteristic lengths L_{sat}, L_{mean}, and L_{BI} from simulations considering partial versus full bleaching conditions.

Our simulations highlight fundamental differences in behavior between saturation, bleaching and mean signals, which make them complementary proxies. Unless very long storage times are considered (>100 Kyr), saturation only decreases longitudinally and can be seen as a passive marker that reflects transport conditions in the absence of lateral supply of saturated grains (Guyez, Bonnet, Reimann, Carretier, & Wallinga, 2022). On the other hand, the longitudinal evolution of bleaching and mean D_e not only reflect transport conditions but also depends on storage in the floodplain, which make them reactive markers. For example, when some bleached grains are buried such that their signal builds up to 10 Gy or more, it decreases the proportion of bleached grains, resulting in a more gradual longitudinal increase in the percentage of bleached grains, that is, in higher L_{Bl}. Similarly, regeneration during storage will affect the mean D_e and therefore the L_{mean}.

5.1.2. Partial Bleaching Conditions

In the way we implement it in the model, partial bleaching has the same effect on the proportion of saturated grains in the river as full bleaching, and consequently partial versus full bleaching results in similar L_{sat} values (Figures 6b and 6c). However, by limiting the drop in D_e value related to P_{Bl}, partial bleaching slows down the downward increase in percentage of bleached grains, resulting in longer L_{Bl} values (Figure 6c). In concert, the mean dose of sediments also decreased more slowly, resulting in longer L_{mean} values than under full bleaching conditions (Figure 6c).

5.2. Comparison Between Natural and Simulated Data

Our model of loss or gain of luminescence signal in response to episodic transport shows similar longitudinal patterns of luminescence signals as those observed along the Waimakariri and Rakaia in the CP. To evaluate the performance of simulations in reproducing these data and identify simulation parameters $<L_T>$, P_{Bl}, and $<R_t>$ that provide results that resemble them most closely, we used a Chi-square test between natural and simulated characteristic distance data (L_{Bl}, L_{sat}, and L_{mean}) with the additional constraint of a percentage of saturated grains at the outlet of $1 \pm 1\%$, as observed on the Waimakariri and Rakaia rivers ($y_0 = 1 \pm 1\%$ in Equation 2).

Under full bleaching conditions, the lowest Chi-square obtained for our 1,036 simulations is 9.52 with six simulation results within 68.3% confidence level (1-sigma confidence interval; Table 2). Simulations involving partial bleaching of the grains give significantly lower Chi-square values, the lowest being 1.04, and 15 simulations give results within the 68.3% confidence level (Table 2). These significantly lower Chi-square values indicate that taking partial bleaching into account allows better reproduction of natural data. This can be illustrated by visually comparing the simulated and natural results (Figure 7). Figure 7c shows for example, that with partial bleaching, the fifteen best-fit simulations all correspond to simulated values of L_{sat}, L_{Bl}, and L_{mean} that are in the range of values fitted to the field data (see also Table 2). In contrast, the best-fit simulations for full bleaching conditions provide no solutions where all three parameters are inside the range of values fitted to the field data (Figure 7b, Table 2). In general, we observe that models with full bleaching fail in reproducing the data because they always give values of L_{sat}, L_{Bl}, and L_{mean} that are very close, all in the same range. In contrast, on the rivers studied here, the values of L_{Bl} are three to four times higher than L_{sat}, that is, longitudinally, the number of bleached grains increases more slowly than the decrease in the number of saturated ones. Only simulations with partial bleaching allow decoupling the longitudinal trends of saturation and bleaching. Only these will thus be considered in the following discussion.

6. Discussion: Insight Into Transport and Storage on the Waimakariri and Rakaia Rivers From Luminescence

The 15 simulations of the partial bleaching model that best perform in simulating the Waimakariri and Rakaia data correspond to a set of combinations of input parameters $<L_T>$, P_{Bl}, and $<R_t>$ with a large range of values (Table 2). Together, these input parameters draw a planar surface in a 3D $<L_T>-P_{Bl}-<R_t>$ space (Figure 8), which illustrates that multiple combinations of parameters can explain our observations in the natural systems. Overall, we observe a trade-off between the transfer length $<L_T>$ and the bleaching probability P_{Bl} because long $<L_T>$ necessarily implies high bleaching efficiency to fit the data. We also observe that high P_{Bl} values allow almost all the $<R_t>$ that we considered, from 1 to 800 yrs, contrary to low P_{Bl} values that are only associated with short $<R_t>$. Indeed, it seems that when bleaching is very efficient, any dose acquired during $<R_t>$ is most likely bleached during the following transport event. Thus, when P_{Bl}, is high, the storage history of the grains has

Table 2
List of the Input Parameters and Results From Simulations That Best Explain Data From the Rakaia and Waimakariri Rivers Considering a Chi-Square Test at 1-Sigmas for the Full Bleaching and Partial Bleaching Models

Model	$<L_T>$ (km)	$<R_f>$ (yrs)	P_{BI} (−)	Residence time (yrs)	River length (km)	Virtual velocity (m/yr)	L_{sat} (km)	L_{mean} (km)	L_{BI} (km)	Chi-2
Full bleaching	*4*	*100*	*0.125*	*5,200*	*200*	*38.5*	*27.5 ± 0.6*	*25.5 ± 1.4*	*29.3 ± 0.8*	*9.52*
	4	*20*	*0.125*	*980*	*200*	*204.1*	*28.4 ± 0.8*	*25.0 ± 0.6*	*31.1 ± 0.4*	*9.87*
	7.5	*100*	*0.25*	*5,479*	*400*	*73*	*26.8 ± 0.9*	*26.2 ± 0.9*	*29.8 ± 0.5*	*9.92*
	7.5	*20*	*0.30*	*1,094*	*400*	*365.6*	*25.3 ± 0.6*	*26.0 ± 0.9*	*28.1 ± 0.6*	*10.14*
	3	*2*	*0.10*	*199*	*200*	*1,005*	*28.8 ± 0.6*	*23.7 ± 0.9*	*29.9 ± 0.6*	*10.52*
	2	*20*	*0.075*	*2,135*	*200*	*93.7*	*24.6 ± 0.3*	*22.7 ± 1*	*27.6 ± 0.4*	*10.52*
Partial bleaching	2	100	0.075	9,908	200	20.2	25.7 ± 0.6	89.5 ± 4.5	96 ± 3.8	1.04
	7.5	100	0.25	5,668	400	70.6	25.2 ± 0.6	81.4 ± 2.3	94.1 ± 1.4	1.08
	3	150	0.125	10,259	200	19.5	25.9 ± 0.9	75.3 ± 2.5	91 ± 3.3	1.35
	7.5	*300*	*0.30*	*16,633*	*400*	*24*	*26.0 ± 0.6*	*77.4 ± 3.7*	*88.8 ± 2.6*	*1.47*
	2	50	0.075	5,047	200	39.6	23.9 ± 0.5	81.3 ± 4.3	84.3 ± 1.2	1.52
	10	*800*	*0.40*	*35,038*	*400*	*11.4*	*25.1 ± 0.8*	*68.0 ± 2.6*	*79.8 ± 3.5*	*1.6*
	7.5	*400*	*0.30*	*21,899*	*400*	*18.3*	*24.7 ± 0.4*	*65.4 ± 2.5*	*82.2 ± 2.3*	*1.72*
	2	20	0.075	2,128	200	94	25.0 ± 0.4	84.5 ± 5.3	83.5 ± 1.3	1.74
	5	100	0.20	8,167	400	49	26.9 ± 0.4	77.5 ± 2.7	85.9 ± 1.6	1.81
	5	*200*	*0.20*	*17,515*	*400*	*22.8*	*23.8 ± 0.3*	*76.9 ± 5.3*	*81.7 ± 2.3*	1.82
	15	*800*	*0.50*	*21,720*	*400*	*18.4*	*28.1 ± 1.6*	*78.0 ± 3.4*	*99.3 ± 4.6*	*1.88*
	20	*20*	*0.50*	*442*	*400*	*905*	*28.7 ± 1.7*	*92.2 ± 2.5*	*111.7 ± 2.5*	1.94
	3	100	0.125	7,032	200	28.4	25.1 ± 0.5	74.8 ± 4.3	77.5 ± 1	1.96
	0.5	*20*	*0.02*	*4,191*	*100*	*23.9*	*25.9 ± 0.5*	*97.8 ± 13.4*	*90.5 ± 2.5*	1.97
	15	*2*	*0.50*	*83*	*400*	*4819.3*	*27.1 ± 1.5*	*62.9 ± 1.9*	*82 ± 1.7*	1.99

Note. Lines in italic are simulations whose results are however hardly conceivable with regard to setting (see text).

a minor influence on longitudinal data, because of the efficient "erasing power" of bleaching. This effect does not apply to simulations with low P_{BI}, which only succeed in reproducing data for low $<R_f>$ values (Figure 8).

Although the fifteen best-fit simulations all statistically represent valid solutions to reproduce natural data, some combinations of parameters are more difficult to conciliate with the context of the Waimakariri and Rakaia rivers, than others. We discuss in the following the relevance of model parameters $<L_T>$ and $<R_f>$ in this context. First, regarding transport distances, $<L_T>$ values in our best-fit simulation range from 0.5 to 20 km (Figure 8 and Table 2).

As a reminder, in each simulation $<L_T>$ is the mean of all grain displacements (see Section 4). The distribution of these event transport distances is positively skewed (Figure 9a), with a lower median value than the mean and some maximum values that exceed 100 km in the simulations with the $<L_T>$ of 15–20 km. In braided rivers, sediment travel length over a single flood event is estimated to be first order by considering the distance between confluence-bifurcation couplets (Kasprak et al., 2015; Pryce & Ashmore, 2003). This distance is about 0.5–1 km for the Rakaia and Waimakariri rivers (Carson & Griffiths, 1989; Hundey & Ashmore, 2009; Pryce & Ashmore, 2003) and in principle, it could be considered here as a basis for discussing the relevance of the best-fit simulations. These gravel-bed rivers have a median diameter D_{50} of about 25–30 mm (Hundey & Ashmore, 2009), significantly larger than the grain size used for our analysis, so we can assume that most travel distances of our particles are longer than 0.5–1 km (Church & Hassan, 1992). However, we assume that it does not exceed this range too much because changes between erosion and deposition related to braided patterns (Kasprak et al., 2015) influence transport and redeposition of the majority of grain sizes. Sandy layers in coarse grained braided systems are indeed found in chute channels and bar tails (Bluck, 1979), where all our samples were obtained (see Figure 2 and Figures S1 and S2 in Supporting Information S1). Thus, we propose to exclude simulations with the highest

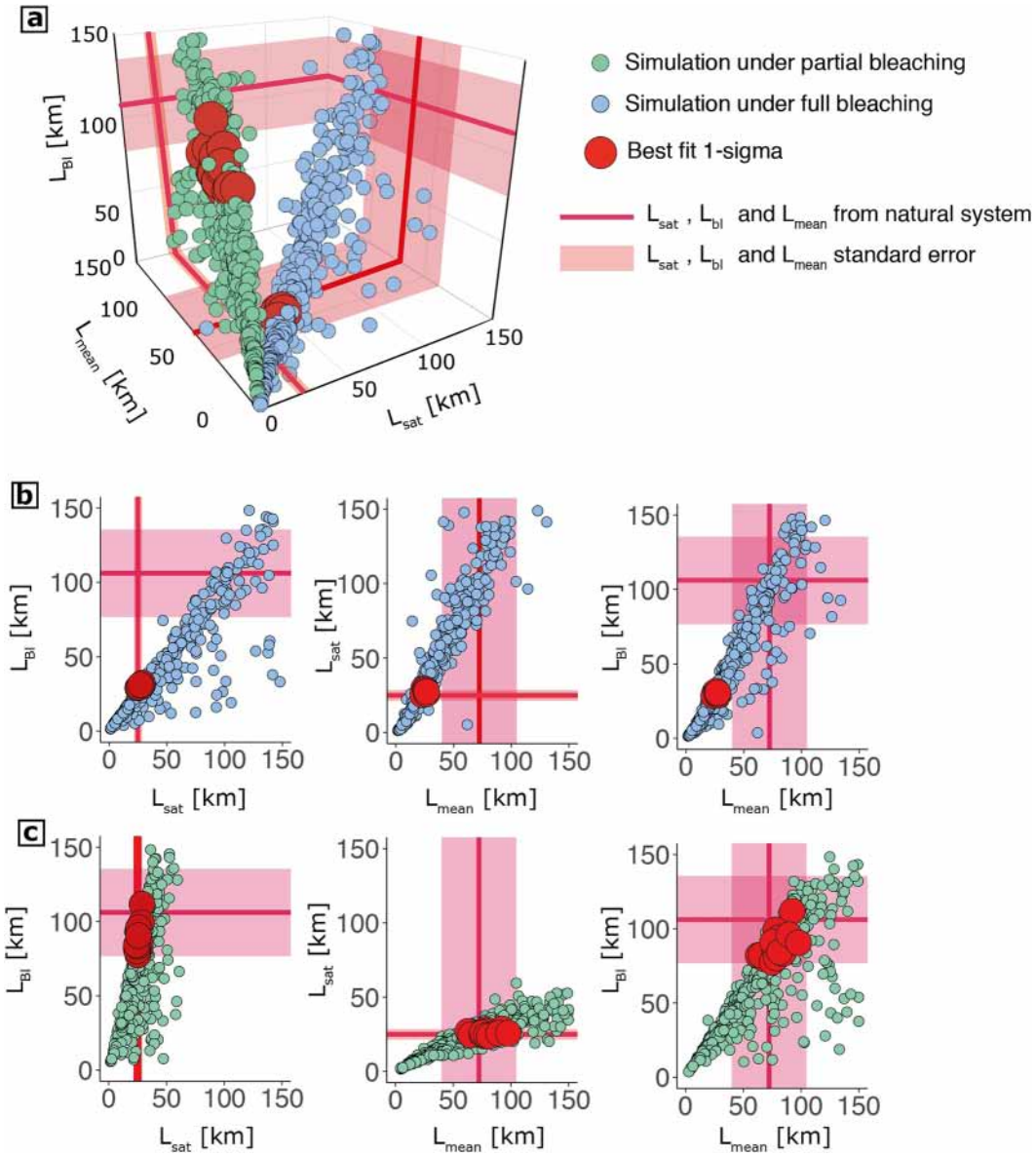

Figure 7. Graphical representation of characteristic lengths L_{sat}, L_{mean}, and L_{Bl} calculated from simulations and comparison with natural values (L_{Bl} = 106.12 ± 29.33 km, L_{sat} = 24.93 ± 3.54 km, and L_{mean} = 72.29 ± 32.35 km). The characteristic lengths measured on natural system data are shown with the red lines and their standard errors with pink area. (a) 3D plot of data under full (blue circles) or partial (green circles) bleaching conditions. For each data set, red symbols show best-fit data (Chi-square test, simulation results within 68.3% confidence level; see text). (b) 2D plots of simulation results under full bleaching conditions. (c) 2D plots of simulation results under partial bleaching conditions. See text for comments.

$<L_T>$ of 15–20 km, which are characterized by a median of 8–13 km (Figure 9a), which are quite high distances compared to the size of the braided elements of the Waimakariri and Rakaia rivers. In the same way, the median of transport length distribution for the best-fit simulation with the lowest $<L_T>$ of 0.5 km is 0.3 km (Figure 9a), so we also suggest that this simulation is not relevant to the studied rivers. To conclude, among the fifteen best-fit simulations, we propose to restrain the preferred solutions to simulations with mean transport distances $<L_T>$ between 2 and 10 km, for which the majority of unit transport distances at the event transport scale are respectively of 0.4–2.0 km (Figure 9a).

Regarding resting times $<R_t>$, the fifteen best-fit simulations show a large range of values, from 2 to 800 yrs (Figure 8 and Table 2). Here again, we recall here that for each simulation, $<R_t>$ is the mean of event-scale values whose distribution is positively skewed with a long tail, with maxima that exceed 10^5 years in some simulations

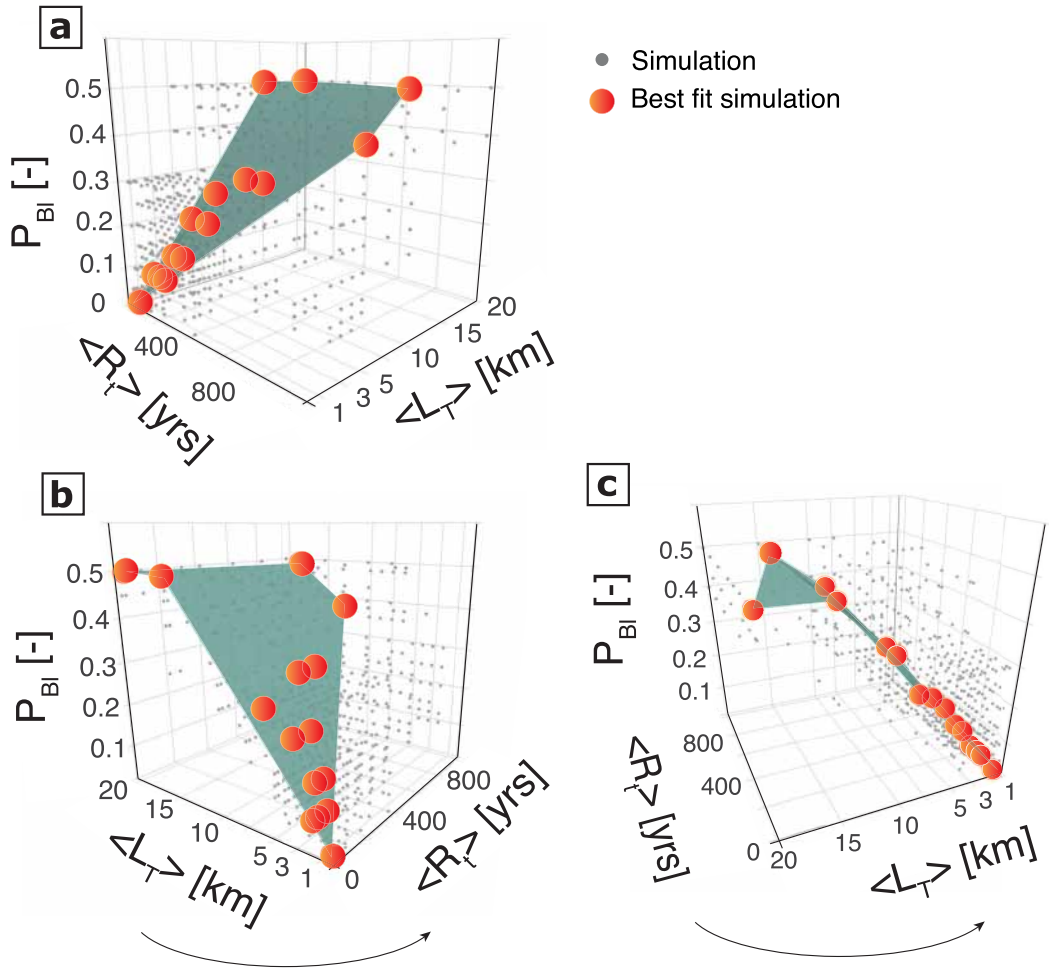

Figure 8. Graphical representation in 3D-space of input parameters $<R_t>$, P_{BI}, and $<L_T>$ of all the 555 simulations (gray dots) performed under partial bleaching conditions. Simulations that succeed in reproducing natural data (Chi-square test, simulation results within 68.3% confidence level) are shown by red balls. A plane drawn by interpolating these best-fit data is shown in green colors.

(Figure 9b). Although the resting times of particles in the Rakaia and Waimakariri floodplains are unknown, evidence suggests that simulations with the longest $<R_t>$ values hardly apply to rivers in the CP. Reinfelds and Nanson (1993) estimate, for example, that the Waimakariri River is capable of reworking its entire floodplain over a period of 250 yrs, including the remobilization of vegetated surfaces developed at 30–50 yrs timescale. Indeed, at a scale of 20–30 years, comparison between satellite time series and aerial views of the rivers shows that some bars in the floodplain are vegetated and that at the same time, some vegetated bars are reworked. This implies that a non-negligible number of grains spends several decades in the floodplain between two transportation events, as also proposed by Reinfelds and Nanson (1993). However, the studied rivers are very mobile at the annual scale (Lane et al., 2003) and the exceptionally high load that they carry (3–4 Mt/yr; Griffiths, 1981) indicates a very high transport capacity. This suggests that most grains are remobilized in the floodplain at a time-scale that ranges from a year to several decades. On this basis, we propose that the three best-fit simulations with the longest mean resting time $<R_t>$ of 200–800 yrs are not representative, given the median of their storage time distribution longer than 100 yrs (Figure 9b). The same conclusion arises if one considers the mean residence time of particles in these simulations (Table 2), estimated from the cumulative time that each grain spends in storage in the floodplains, with regard to geological constraints on the development of the river floodplain. For simulations with $<R_t>$ of 200–800 yrs, the mean residence times of the grains in the floodplain range from 16 to 35 Kyr, respectively (Table 2), which are regarded unlikely. This is indeed of the same order as the age of the upper deposits of the CP in which the Rakaia and Waimakariri are entrenched (18–37 Kyr: Rowan et al., 2012). Thus, in the following we propose to exclude the best-fit simulations with longest $<R_t>$ of 200–800 years.

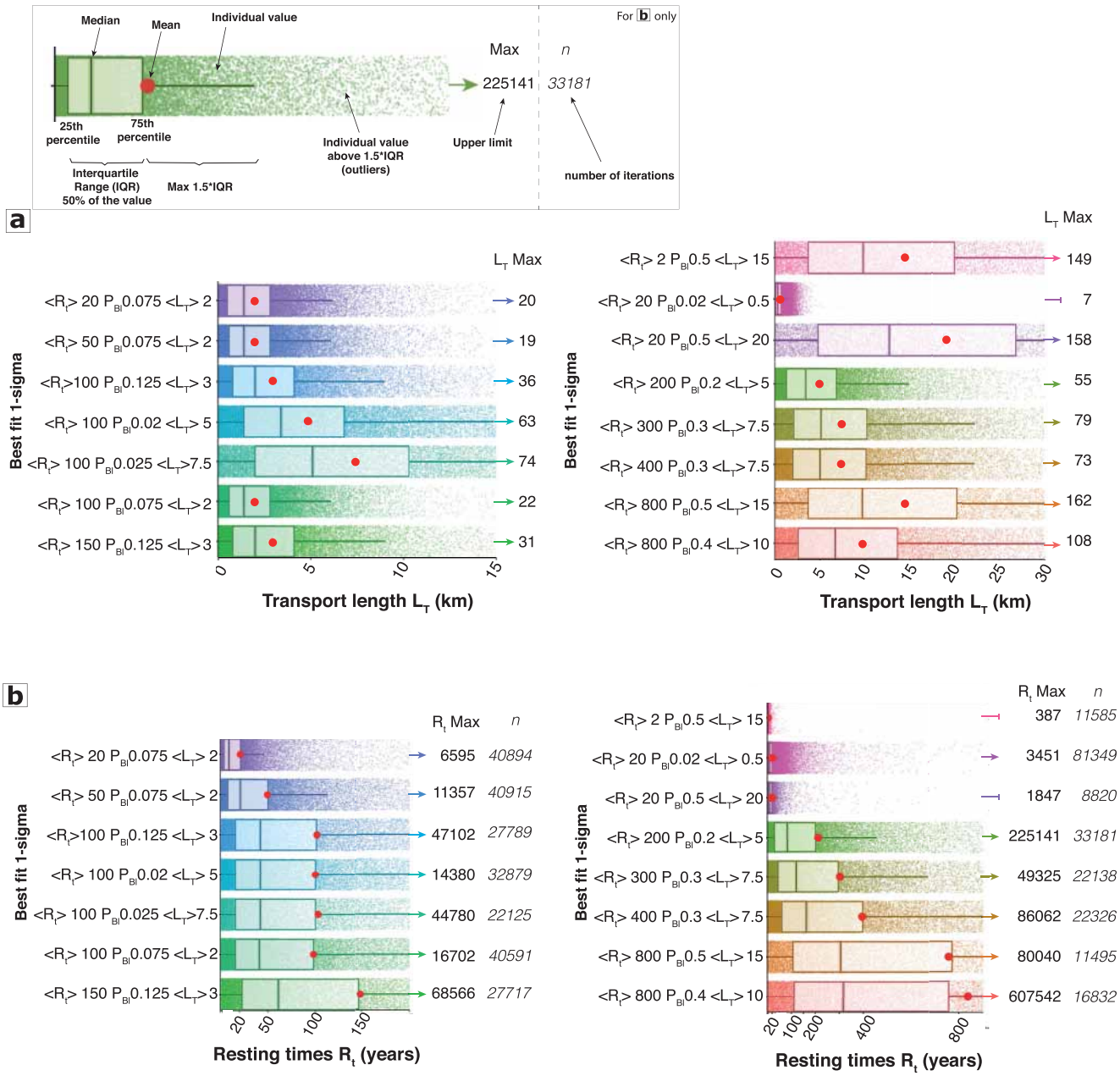

Figure 9. The distribution of (a) event scale transport length L_T and (b) resting time R_t of the 15 best-fit simulations (Chi-square test, simulation results within 68.3% confidence level). On (a) and on (b) the left column shows the distributions that were accepted and the right column shows the ones that were excluded in the discussion (see insets for legend).

On the basis of the above discussion, among the fifteen best-fit simulations, we propose to exclude those with the highest values of $<L_T>$ and $<R_t>$ because we consider them likely not consistent with the setting. As explained previously, best-fit simulations with the high values of $<L_T>$ and $<R_t>$ only succeeded in reproducing data because of the systematic association to very good bleaching conditions, that is, to high values of P_{BI}. In fact, discarding the best-fit simulations with high values of $<L_T>$ and $<R_t>$ thus excludes all solutions with the highest P_{BI} values of 0.4–0.5 (Figure 8). This supports our hypothesis that such high P_{BI} values are unrealistic for fluvial settings, where poor bleaching is commonly observed (Wallinga, 2002). Whether this range of P_{BI} values is specific to braided systems and could still be applied for rivers with different fluvial styles, as well as in contexts of lower sediment flux, would however deserve to be considered in future studies.

Finally, the mean residence times of the seven remaining best-fit simulations vary from 2.1 to 10.3 Kyr (Table 2), with a mean value of ~6.9 ± 2.9 Kyrs. It corresponds to mean virtual transit velocities of 20–95 m.yr^{-1} (Table 2), with a mean value of 46 ± 28 m.yr^{-1}. This range of values is lower than virtual transit velocities estimated using cosmogenic isotopes in the study by Repasch et al. (2020). In the upstream part of the Rio Bermejo (Argentina), also a braided system, they measured virtual velocities of 386 ± 168–586 ± 157 m.yr^{-1}. However, their estimates have been obtained on a system that is much larger (>400 km against ~70 km here) and has much greater sediment flux (104 Mt.yr^{-1} against 3–4 Mt.yr^{-1} here). Whether the difference between our respective estimates is due to the difference in river dynamics and settings or to methods used deserves to be investigated in future work. However, it is encouraging to note that the two methods, although based on completely different approaches, give results within an order of magnitude.

Finally, our estimates are an order of magnitude higher that virtual transit velocities of 1.8 ± 0.1–2.8 ± 0.1 m.yr^{-1} deduced from luminescence by Gray et al. (2018) for the South River (USA). Again, this river is in a very different setting and has a very different river style (gently sloping meandering river); we can expect different $<L_T>$ and $<R_t>$. The method developed by Gray et al. (2018) is based on multigrain luminescence data and resolves longitudinal bleaching related to transport. The method requires input information on characteristic storage timescales of fine sand, obtained from sediment budgeting and geochronology. The advantage of the method we present here is that it does not require such additional data, which is made possible by the use of single-grain data and the possibility of taking into account different terms in the distribution of the D_e for each sample, each with its own sensitivity to transport and storage. A potential way for improving our approach could be to combine the analysis of single grain D_e distributions (this study and McGuire & Rhodes, 2015b), with the analysis of multiple signals with different bleaching characteristics (e.g., MET-IRSL; McGuire & Rhodes, 2015a; Reimann et al., 2015). Combining both approaches could provide more natural constraints to restrict the range of model solutions. It is worth noting that contrary to our probabilistic approach of the bleaching process, McGuire and Rhodes (2015b) developed a model in which the intensity of bleaching is defined by the duration of grain exposure to sunlight during transport, coupled to a kinetics bleaching law constrained from laboratory data. This approach has the advantage of considering full or partial bleaching in a unique way depending on the duration of grain exposure to sunlight during flooding events. However, this duration is very difficult to evaluate for all grains in transit in a natural river. In the absence of such data and a hydro-sedimentary model, we chose here to simplify the complexity of bleaching during transport by considering only probability, in a similar way as the dimensionless coefficient "*p*" in Bailey and Arnold (2006). Understanding and being able to quantify bleaching in rivers is one of the greatest challenges to push forward the capability of luminescence data to retrieve information on Earth surface processes.

7. Conclusions and Outlook

This study presents a new approach to obtain quantitative insight into fluvial transport and storage in floodplains from luminescence characteristics of fluvial sediments combined with numerical simulations. For this purpose, we provided a first comprehensive data set of the longitudinal distribution of single-grain luminescence signals measured in feldspar from modern fluvial sediments, in the case of the Waimakariri and Rakai braided rivers of New Zealand. Features such as the percentages of saturated and bleached grains and the mean equivalent dose show very similar longitudinal variations, consistent with a progressive bleaching of grain populations during their downstream transport. Using an original numerical model, we show that the longitudinal evolution of saturation, bleaching and mean equivalent dose are related to fluvial transport and temporary storage in floodplains. This model simulates the progressive bleaching and/or regeneration of the luminescence signal of grains in response to successive steps of fluvial transport and storage in the floodplain, considering two different bleaching dynamics of the grains depending on whether they are fully or only partially bleached. The model succeeds in qualitatively reproducing the observations by using a range of forcing parameters within boundaries that seem realistic for the systems of interest. From a comparison between model outputs and observations, we show that the model is able to reproduce natural data only when partial bleaching is taken into account and under a restricted range of combinations of sediment transfer length, storage duration in the floodplain and bleaching efficiency. From this approach, we show sediment transfer in the investigated rivers may take place at a time scale of 2.1–10.3 Kyr, with a mean value of ~6.9 ± 2.9 Kyr, which corresponds to mean virtual transit velocities of 20–95 m.yr^{-1}, with a mean value of 46 ± 28 m.yr^{-1}.

We expect our approach to be applicable to other river systems, and to open new opportunities to investigate sediment transport, transit and storage. A next step will be to test our model on other geomorphic, tectonic and climatic settings and for different river patterns, with distinct storage dynamics, which requires the acquisition of stream single-grain luminescence data from such systems. With regard to the model, we suggest that further improvement with respect to partial bleaching and scaling of bleaching with transfer length should be prioritized.

Data Availability Statement

Data used for model evaluations can be found in Table 1. Raw data that were used to calculate the data found in Table 1 are available on the Zenodo Data Publisher platform https://doi.org/10.5281/zenodo.7125031 (Guyez, Bonnet, Reimann, Wallinga, & Carretier, 2022).

Acknowledgments
This study was funded by the Franco-Dutch Hubert Curien Partnership (Van Gogh Programme N° VGP.19/00012), CNRS-INSU TelluS-SYSTER Programme (to S. Bonnet) and Franco-German ANR-DFG research project WEARING_DOWN (ANR-21-CE01-0020-01 and DFG RE 3580/2-1). We thank Alice van der Broek-Versendaal and Erna Voskuilen for laboratory support. Reviews and comments by Editor Mikael Attal, Associate Editor Harrison Gray, Rebecca Hodge and two anonymous reviewers improved the manuscript.

References

Adams, J. (1980). Contemporary uplift and erosion of the Southern Alps, New Zealand. *GSA Bulletin*, *91*(1_Part_II), 1–114. https://doi.org/10.1130/GSAB-P2-91-1

Aitken, M. J. (1998). *Introduction to optical dating: The dating of quaternary sediments by the use of photon-stimulated luminescence*. Clarendon Press.

Allen, P. A. (2008). From landscapes into geological history. *Nature*, *451*(7176), 274–276. https://doi.org/10.1038/nature06586

Bailey, R. M., & Arnold, L. J. (2006). Statistical modelling of single grain quartz De distributions and an assessment of procedures for estimating burial dose. *Quaternary Science Reviews*, *25*(19–20), 2475–2502. https://doi.org/10.1016/j.quascirev.2005.09.012

Barrell, D. J. A., Andersen, B. G., & Denton, G. H. (2011). *Glacial geomorphology of the central South Island (GNS science monographs 27)*. Lower Hutt: GNS Science.

Beavan, J., Denys, P., Denham, M., Hager, B., Herring, T., & Molnar, P. (2010). Distribution of present-day vertical deformation across the Southern Alps, New Zealand, from 10 years of GPS data. *Geophysical Research Letters*, *37*(16), L16305. https://doi.org/10.1029/2010gl044165

Berger, G. W. (1990). Effectiveness of natural zeroing of the thermoluminescence in sediments. *Journal of Geophysical Research*, *95*(B8), 12375. https://doi.org/10.1029/JB095iB08p12375

Bluck, B. J. (1979). Structure of coarse grained braided stream alluvium. *Earth and Environmental Science Transactions of the Royal Society of Edinburgh*, *70*(10–12), 181–221. https://doi.org/10.1017/s0080456800012795

Bonnet, S., Reimann, T., Wallinga, J., Lague, D., Davy, P., & Lacoste, A. (2019). Landscape dynamics revealed by luminescence signals of feldspars from fluvial terraces. *Scientific Reports*, *9*(1), 8569. https://doi.org/10.1038/s41598-019-44533-4

Bøtter-Jensen, L., Andersen, C. E., Duller, G. A., & Murray, A. S. (2003). Developments in radiation, stimulation and observation facilities in luminescence measurements. *Radiation Measurements*, *37*(4–5), 535–541. https://doi.org/10.1016/s1350-4487(03)00020-9

Bradley, D. N. (2017). Direct observation of heavy-tailed storage times of bed load tracer particles causing anomalous superdiffusion. *Geophysical Research Letters*, *44*(24), 12–227. https://doi.org/10.1002/2017gl075045

Browne, G. H., & Naish, T. R. (2003). Facies development and sequence architecture of a late quaternary fluvial-marine transition, Canterbury Plains and shelf, New Zealand: Implications for forced regressive deposits. *Sedimentary Geology*, *158*(1–2), 57–86. https://doi.org/10.1016/S0037-0738(02)00258-0

Carretier, S., Guerit, L., Harries, R., Regard, V., Maffre, P., & Bonnet, S. (2020). The distribution of sediment residence times at the foot of mountains and its implications for proxies recorded in sedimentary basins. *Earth and Planetary Science Letters*, *546*, 116448. https://doi.org/10.1016/j.epsl.2020.116448

Carretier, S., & Regard, V. (2011). Is it possible to quantify pebble abrasion and velocity in rivers using terrestrial cosmogenic nuclides? *Journal of Geophysical Research*, *116*(F4), F04003. https://doi.org/10.1029/2011jf001968

Carretier, S., Regard, V., Leanni, L., & Farias, M. (2019). Long-term dispersion of river gravel in a canyon in the Atacama Desert, Central Andes, deduced from their ^{10}Be concentrations. *Scientific Reports*, *9*(1), 1–12. https://doi.org/10.1038/s41598-019-53806-x

Carson, M. A., & Griffiths, G. A. (1989). Gravel transport in the braided Waimakariri River: Mechanisms, measurements and predictions. *Journal of Hydrology*, *109*(3–4), 201–220. https://doi.org/10.1016/0022-1694(89)90016-4

Chamberlain, E. L., & Wallinga, J. (2019). Seeking enlightenment of fluvial sediment pathways by optically stimulated luminescence signal bleaching of river sediments and deltaic deposits. *Earth Surface Dynamics*, *7*(3), 723–736. https://doi.org/10.5194/esurf-7-723-2019

Chamberlain, E. L., Wallinga, J., & Shen, Z. (2018). Luminescence age modeling of variably-bleached sediment: Model selection and input. *Radiation Measurements*, *120*, 221–227. https://doi.org/10.1016/j.radmeas.2018.06.007

Church, M., & Hassan, M. A. (1992). Size and distance of travel of unconstrained clasts on a streambed. *Water Resources Research*, *28*(1), 299–303. https://doi.org/10.1029/91wr02523

Cox, S., & Barrell, D. (2007). Geology of the Aoraki area 1: 250,000, geological map 15 *GNS Science*. *GNS Science*, *1*.

Davies-Colley, R. J., & Nagels, J. W. (2008). Predicting light penetration into river waters. *Journal of Geophysical Research*, *113*(G3), G03028. https://doi.org/10.1029/2008JG000722

Davy, P., Croissant, T., & Lague, D. (2017). A precipiton method to calculate river hydrodynamics, with applications to flood prediction, landscape evolution models, and braiding instabilities. *Journal of Geophysical Research: Earth Surface*, *122*(8), 1491–1512. https://doi.org/10.1002/2016jf004156

Davy, P., & Lague, D. (2009). Fluvial erosion/transport equation of landscape evolution models revisited. *Journal of Geophysical Research*, *114*(F3), F03007. https://doi.org/10.1029/2008JF001146

Ditlefsen, C. (1992). Bleaching of K-feldspars in turbid water suspensions: A comparison of photo- and thermoluminescence signals. *Quaternary Science Reviews*, *11*(1–2), 33–38. https://doi.org/10.1016/0277-3791(92)90039-B

Dosseto, A., Bourdon, B., Gaillardet, J., Maurice-Bourgoin, L., & Allegre, C. J. (2006). Weathering and transport of sediments in the Bolivian Andes: Time constraints from uranium-series isotopes. *Earth and Planetary Science Letters*, *248*(3–4), 759–771. https://doi.org/10.1016/j.epsl.2006.06.027

Fülöp, R.-H., Codilean, A. T., Wilcken, K. M., Cohen, T. J., Fink, D., Smith, A. M., et al. (2020). Million-year lag times in a post-orogenic sediment conveyor. *Science Advances*, *6*(25), eaaz8845. https://doi.org/10.1126/sciadv.aaz8845

Godfrey-Smith, D. I., Huntley, D. J., & Chen, W.-H. (1988). Optical dating studies of quartz and feldspar sediment extracts. *Quaternary Science Reviews*, *7*(3–4), 373–380. https://doi.org/10.1016/0277-3791(88)90032-7

Goehring, B. M., Brown, N., Moon, S., & Blisniuk, K. (2021). The transport history of alluvial fan sediment inferred from multiple geochronometers. *Journal of Geophysical Research: Earth Surface*, *126*(9), e2021JF006096. https://doi.org/10.1029/2021jf006096

Gray, H. J., Jain, M., Sawakuchi, A. O., Mahan, S. A., & Tucker, G. E. (2019). Luminescence as a sediment tracer and provenance tool. *Reviews of Geophysics*, *57*(3), 987–1017. https://doi.org/10.1029/2019RG000646

Gray, H. J., & Mahan, S. A. (2015). Variables and potential models for the bleaching of luminescence signals in fluvial environments. *Quaternary International*, *362*, 42–49. https://doi.org/10.1016/j.quaint.2014.11.007

Gray, H. J., Tucker, G. E., & Mahan, S. A. (2018). Application of a luminescence-based sediment transport model. *Geophysical Research Letters*, *45*, 6071–6080. https://doi.org/10.1029/2018GL078210

Griffiths, G. A. (1981). Some suspended sediment yields from south island catchments, New Zealand. *Journal of the American Water Resources Association*, *17*(4), 662–671. https://doi.org/10.1111/j.1752-1688.1981.tb01274.x

Guerit, L., Yuan, X.-P., Carretier, S., Bonnet, S., Rohais, S., Braun, J., & Rouby, D. (2019). Fluvial landscape evolution controlled by the sediment deposition coefficient: Estimation from experimental and natural landscapes. *Geology*, *47*(9), 853–856. https://doi.org/10.1130/G46356.1

Guyez, A., Bonnet, S., Reimann, T., Carretier, S., & Wallinga, J. (2022). Illuminating past river incision, sediment source and pathways using luminescence signals of individual feldspar grains (Rangitikei River, New Zealand). *Earth Surface Processes and Landforms*, *47*(8), 1952–1971. https://doi.org/10.1002/esp.5357

Guyez, A., Bonnet, S., Reimann, T., Wallinga, J., & Carretier, S. (2022). Data for novel approach to quantify sediment transfer and storage in rivers with feldspar single-grain pIRIR (version 1.0) [Dataset]. Zenodo. https://doi.org/10.5281/zenodo.7125031

Herman, F., Cox, S. C., & Kamp, P. J. J. (2009). Low-temperature thermochronology and thermokinematic modeling of deformation, exhumation, and development of topography in the central Southern Alps, New Zealand: Thermochronology in Southern Alps faults. *Tectonics*, *28*(5), TC5011. https://doi.org/10.1029/2008TC002367

Hicks, D. M., Shankar, U., McKerchar, A. I., Basher, L., Lynn, I., Page, M., & Jessen, M. (2011). Suspended sediment yields from New Zealand Rivers. *Journal of Hydrology*, *50*(1), 81–142.

Hippe, K., Kober, F., Zeilinger, G., Ivy-Ochs, S., Maden, C., Wacker, L., et al. (2012). Quantifying denudation rates and sediment storage on the eastern Altiplano, Bolivia, using cosmogenic ^{10}Be, ^{26}Al, and in situ ^{14}C. *Geomorphology*, *179*, 58–70. https://doi.org/10.1016/j.geomorph.2012.07.031

Hovius, N., Stark, C. P., & Allen, P. A. (1997). Sediment flux from a mountain belt derived by landslide mapping. *Geology*, *25*(3), 231. https://doi.org/10.1130/0091-7613(1997)025<0231:SFFAMB>2.3.CO;2

Hundey, E. J., & Ashmore, P. E. (2009). Length scale of braided river morphology. *Water Resources Research*, *45*(8), W08409. https://doi.org/10.1029/2008wr007521

Jerolmack, D. J., & Paola, C. (2010). Shredding of environmental signals by sediment transport. *Geophysical Research Letters*, *37*(19), L19401. https://doi.org/10.1029/2010gl044638

Kamp, P. J., & Tippett, J. M. (1993). Dynamics of Pacific plate crust in the South Island (New Zealand) zone of oblique continent-continent convergence. *Journal of Geophysical Research*, *98*(B9), 16105–16118. https://doi.org/10.1029/93jb01091

Kars, R. H., Reimann, T., Ankjaergaard, C., & Wallinga, J. (2014). Bleaching of the post-IR IRSL signal: New insights for feldspar luminescence dating: Feldspar luminescence dating. *Boreas*, *43*(4), 780–791. https://doi.org/10.1111/bor.12082

Kasprak, A., Wheaton, J. M., Ashmore, P. E., Hensleigh, J. W., & Peirce, S. (2015). The relationship between particle travel distance and channel morphology: Results from physical models of braided rivers. *Journal of Geophysical Research: Earth Surface*, *120*(1), 55–74. https://doi.org/10.1002/2014JF003310

Laity, J. (2003). Aeolian destabilization along the Mojave River, Mojave Desert, California: Linkages among fluvial, groundwater, and aeolian systems. *Physical Geography*, *24*(3), 196–221. https://doi.org/10.2747/0272-3646.24.3.196

Lajeunesse, E., Malverti, L., & Charru, F. (2010). Bed load transport in turbulent flow at the grain scale: Experiments and modeling. *Journal of Geophysical Research*, *115*(F4), F04001. https://doi.org/10.1029/2009jf001628

Lane, S. N., Westaway, R. M., & Murray Hicks, D. (2003). Estimation of erosion and deposition volumes in a large, gravel-bed, braided river using synoptic remote sensing. *Earth Surface Processes and Landforms: The Journal of the British Geomorphological Research Group*, *28*(3), 249–271. https://doi.org/10.1002/esp.483

Liu, B., & Coulthard, T. J. (2017). Modelling the interaction of aeolian and fluvial processes with a combined cellular model of sand dunes and river systems. *Computers & Geosciences*, *106*, 1–9. https://doi.org/10.1016/j.cageo.2017.05.003

Martin, A. N., Dosseto, A., May, J.-H., Jansen, J. D., Kinsley, L. P., & Chivas, A. R. (2019). Sediment residence times in catchments draining to the Gulf of Carpentaria, northern Australia, inferred by uranium comminution dating. *Geochimica et Cosmochimica Acta*, *244*, 264–291. https://doi.org/10.1016/j.gca.2018.09.031

McGuire, C., & Rhodes, E. J. (2015a). Determining fluvial sediment virtual velocity on the Mojave River using K-feldspar IRSL: Initial assessment. *Quaternary International*, *362*, 124–131. https://doi.org/10.1016/j.quaint.2014.07.055

McGuire, C., & Rhodes, E. J. (2015b). Downstream MET-IRSL single-grain distributions in the Mojave River, southern California: Testing assumptions of a virtual velocity model. *Quaternary Geochronology*, *30*, 239–244. https://doi.org/10.1016/j.quageo.2015.02.004

Métivier, F., Gaudemer, Y., Tapponnier, P., & Klein, M. (1999). Mass accumulation rates in Asia during the Cenozoic. *Geophysical Journal International*, *137*(2), 280–318. https://doi.org/10.1046/j.1365-246x.1999.00802.x

Mey, J., Schwanghart, W., de Boer, A.-M., & Reimann, T. (2020). Illuminating the speed of sand–quantifying sediment transport using optically stimulated luminescence. In *Copernicus meetings*.

Mosley, M. P. (1983). Response of braided rivers to changing discharge. *Journal of Hydrology*, 18–67.

Murray, A. S., & Roberts, R. G. (1997). Determining the burial time of single grains of quartz using optically stimulated luminescence. *Earth and Planetary Science Letters*, *152*(1–4), 163–180. https://doi.org/10.1016/s0012-821x(97)00150-7

Murray, A. S., Thomsen, K. J., Masuda, N., Buylaert, J. P., & Jain, M. (2012). Identifying well-bleached quartz using the different bleaching rates of quartz and feldspar luminescence signals. *Radiation Measurements*, *47*(9), 688–695. https://doi.org/10.1016/j.radmeas.2012.05.006

Nichols, K. K., Bierman, P. R., Caffee, M., Finkel, R., & Larsen, J. (2005). Cosmogenically enabled sediment budgeting. *Geology*, *33*(2), 133–136. https://doi.org/10.1130/g21006.1

Norris, R. J., & Cooper, A. F. (2001). Late quaternary slip rates and slip partitioning on the Alpine Fault, New Zealand. *Journal of Structural Geology*, *23*(2–3), 507–520. https://doi.org/10.1016/s0191-8141(00)00122-x

Preusser, F., Degering, D., Fuchs, M., Hilgers, A., Kadereit, A., Klasen, N., et al. (2008). Luminescence dating: Basics, methods and applications. *E & G Quaternary Science Journal*, *57*(1/2), 95–149. https://doi.org/10.3285/eg.57.1-2.5

Pryce, R. S., & Ashmore, P. E. (2003). *Bed particle path length distributions and channel morphology in gravel-bed streams* (p. 48). Geography Publications.

Reimann, T., Notenboom, P. D., De Schipper, M. A., & Wallinga, J. (2015). Testing for sufficient signal resetting during sediment transport using a polymineral multiple-signal luminescence approach. *Quaternary Geochronology*, *25*, 26–36. https://doi.org/10.1016/j.quageo.2014.09.002

Reimann, T., Thomsen, K. J., Jain, M., Murray, A. S., & Frechen, M. (2012). Single-grain dating of young sediments using the pIRIR signal from feldspar. *Quaternary Geochronology*, *11*, 28–41. https://doi.org/10.1016/j.quageo.2012.04.016

Reinfelds, I., & Nanson, G. (1993). Formation of braided river floodplains, Waimakariri River, New Zealand. *Sedimentology*, *40*(6), 1113–1127. https://doi.org/10.1111/j.1365-3091.1993.tb01382.x

Repasch, M., Scheingross, J. S., Hovius, N., Lupker, M., Wittmann, H., Haghipour, N., et al. (2021). Fluvial organic carbon cycling regulated by sediment transit time and mineral protection. *Nature Geoscience*, *14*(11), 842–848. https://doi.org/10.1038/s41561-021-00845-7

Repasch, M., Wittmann, H., Scheingross, J. S., Sachse, D., Szupiany, R., Orfeo, O., et al. (2020). Sediment transit time and floodplain storage dynamics in alluvial rivers revealed by meteoric ^{10}Be. *Journal of Geophysical Research: Earth Surface*, *125*(7), e2019JF005419. https://doi.org/10.1029/2019jf005419

Rhodes, E. J., & Leathard, J. A. (2022). MET-IRSL used to track pre-depositional sediment transport history. *Quaternary Geochronology*, *70*, 101294. https://doi.org/10.1016/j.quageo.2022.101294

Rowan, A. V., Roberts, H. M., Jones, M. A., Duller, G. A., Covey-Crump, S. J., & Brocklehurst, S. H. (2012). Optically stimulated luminescence dating of glaciofluvial sediments on the Canterbury Plains, South Island, New Zealand. *Quaternary Geochronology*, *8*, 10–22. https://doi.org/10.1016/j.quageo.2011.11.013

Sinclair, H. D., Stuart, F. M., Mudd, S. M., McCann, L., & Tao, Z. (2019). Detrital cosmogenic ^{21}Ne records decoupling of source-to-sink signals by sediment storage and recycling in Miocene to present rivers of the Great Plains, Nebraska, USA. *Geology*, *47*(1), 3–6. https://doi.org/10.1130/G45391.1

Smedley, R. K., & Skirrow, G. K. (2020). Luminescence dating in fluvial settings: Overcoming the challenge of partial bleaching. In *Palaeohydrology* (pp. 155–168). Springer.

Stokes, S., Bray, H. E., & Blum, M. D. (2001). Optical resetting in large drainage basins: Tests of zeroing assumptions using single-aliquot procedures. *Quaternary Science Reviews*, *7*(5–9), 879–885. https://doi.org/10.1016/s0277-3791(00)00045-7

Straub, K. M., Duller, R. A., Foreman, B. Z., & Hajek, E. A. (2020). Buffered, incomplete, and shredded: The challenges of reading an imperfect stratigraphic record. *Journal of Geophysical Research: Earth Surface*, *125*(3), e2019JF005079. https://doi.org/10.1029/2019jf005079

Trimble, S. W., & Mendel, A. C. (1995). The cow as a geomorphic agent—A critical review. *Geomorphology*, *13*(1–4), 233–253. https://doi.org/10.1016/0169-555x(95)00028-4

Vázquez-Tarrío, D., Recking, A., Liébault, F., Tal, M., & Menéndez-Duarte, R. (2019). Particle transport in gravel-bed rivers: Revisiting passive tracer data. *Earth Surface Processes and Landforms*, *44*(1), 112–128. https://doi.org/10.1002/esp.4484

Wallinga, J. (2002). Optically stimulated luminescence dating of fluvial deposits: A review. *Boreas*, *31*(4), 303–322. https://doi.org/10.1080/030094802320942536

Wintle, A. G., & Murray, A. S. (2006). A review of quartz optically stimulated luminescence characteristics and their relevance in single-aliquot regeneration dating protocols. *Radiation Measurements*, *41*(4), 369–391. https://doi.org/10.1016/j.radmeas.2005.11.001